Flood-Related Extreme Precipitation in Southwestern Germany: Development of a Two-Dimensional Stochastic Precipitation Model

Florian Ehmele[1] and Michael Kunz[1,2]

[1]Institute of Meteorology and Climate Research, Karlsruhe Institute of Technology (KIT), Hermann-von-Helmholtz-Platz 1, 76344 Eggenstein-Leopoldshafen, Germany.
[2]Center for Disaster Management and Risk Reduction Technology (CEDIM), KIT - Karlsruhe, Germany

Correspondence to: Florian Ehmele (florian.ehmele@kit.edu)

Abstract. Various application fields, such as insurance industry risk assessments for the design of flood protection systems, require reliable precipitation statistics in high spatial resolution, including estimates for events with high return periods. Observations from point stations, however, lack spatial representativeness, especially over complex terrain. Thus, they do not reliably represent the heavy tail of the distribution function. Common numerical weather models are not capable of running simulations over thousands of years. This paper presents a new numerical method to simulate larger-scale precipitation fields stochastically, based on a linear theory describing orographic precipitation and additional functions that consider synoptically driven rainfall and embedded convection in a simplified way. The model is initialized by various statistical distribution functions describing prevailing atmospheric conditions, such as wind vector, moisture content, or stability, estimated from radiosonde observations for a limited sample of the 200 strongest rainfall events observed.

The model is applied for the stochastic simulation of heavy rainfall over the complex terrain of Southwest Germany. It is shown that the model, despite its simplicity, yields reliable precipitation fields. Differences between observed and simulated rainfall statistics are small, being in the order of only $\pm 10\,\%$ for return periods of up to 1,000 years.

1 Introduction

Persistent precipitation over large areas and the resulting widespread flooding frequently cause major damage in Central Europe in the order of several billion Euro (EUR) per event. In Germany, two extreme floods in 2002 and 2013 with estimated return periods of more than 200 years (Schröter et al., 2015) collectively caused more than EUR 22 billion in economic losses (inflation adjusted to 2017; MunichRe, 2017). Beside these extreme events, smaller floods with higher frequencies, such as those in 2005, 2006, 2010, and 2011 (Uhlemann et al., 2010; Kienzler et al., 2015), also contribute to the large damage potential associated with floods.

Flood risk estimation, for example, for insurance purposes or for the design of appropriate flood mitigation systems, requires the dependable statistical analysis of extreme rainfall. Traditionally, these extremes have been estimated at point stations from intensity-duration-frequency (IDF) with extreme value statistics being applied (Koutsoyiannis et al., 1998). This method, however, implies two drawbacks: (i) the low spatial representativeness of point observations and (ii) the limited observation period so that not all possible extreme configurations enter the samples. To account for the former shortcoming, either geostatistical

interpolation routines, such as kriging (Goovaerts, 2000), or techniques that relate precipitation to both orographic characteristics and atmospheric parameters (e.g., Basist et al., 1994; Drogue et al., 2002) are used. Shortcomings resulting from these methods are the lack of representativeness of station data with respect to the surroundings, and the neglect of dynamical and thermodynamical processes decisive for real precipitation events. To account for the limited observation period, several studies have employed stochastic weather generators to simulate precipitation events at single grid points (e. g., Richardson, 1981; Furrer and Katz, 2007; Neykov et al., 2014). A recent study by Cross et al. (2017) introduced a censored rainfall modeling approach designed to reduce the underestimation of extremes. Albeit considering the long-term variability of precipitation, which leads to more reliable estimates for extremes, these approaches still lack spatial representativeness.

In the present study, we present a two-dimensional stochastic precipitation model (SPM2D) that allows for simulating a large number of precipitation fields using a high spatial resolution. Large sample sizes of several thousand events are required to obtain robust estimates of the hazard for high recurrence periods, like the one-in-200-year events that have to be considered by insurance companies. Common numerical weather models are not capable of simulating thousands of years due to their complexity and the resulting long computation time.

The core of our SPM2D is the diagnostic linear model approach for orographic precipitation according to Smith and Barstad (2004). The model considers wave dynamics in terms of the linearized equations of a stratified, non-hydrostatic flow over mountains (Smith, 1980). Input parameters are atmospheric flow quantities connected to precipitation, such as stability, moisture scaling height, precipitable water, or flow speed, all estimated from radiosoundings. Additional internal free parameters, such as characteristic time scales for cloud water conversion and fallout, serve as calibration parameters. The Smith and Barstad (2004) model has been successfully applied in various regions: e. g. several locations in the United States (Barstad and Smith, 2005), Iceland (Crochet et al., 2007), Southwest Germany (Kunz, 2011), or Southern and Northern Norway (Caroletti and Barstad, 2010; Barstad and Caroletti, 2013). Despite the fact that characteristic time scales and background precipitation may vary from one situation to another, it is found that simulations using fixed values for the free parameters yield trustworthy results. In our approach, we added two additional components to the orographic and background precipitation: synoptic-scale fronts and convection embedded into mainly stratiform clouds (Fuhrer and Schär, 2005). Whereas the former component may enhance (or reduce in case of absence) precipitation over larger areas, the latter may lead to locally slightly enhanced totals.

In the present study, we applied the SPM2D to both single historical events with heavy rainfall (training events) and over a long-term period of several thousand years (validation events). In the latter case, the required model parameters are estimated from probability density functions (pdfs) and are stochastically selected. In this application, we fixed the internal free parameters to constant values estimated by thorough calibration. Because precipitation regimes in summer and winter vary significantly, we seasonally differentiate our analyses.

The investigation area for this study is the Federal State of Baden-Württemberg (BW) in Southwest Germany, which extends from 46.6 to 50.8° N and from 6.9 to 11.1° E (Fig. 1). The terrain exhibits a certain degree of complexity: with the broad Rhine Valley with elevations of 100–200 m bounded by the Vosges Mountains (France) to the west and the Black Forest mountains to the east; with a maximum elevation of 1493 m (Feldberg) in Southern Black Forest; and with some rolling terrain to the

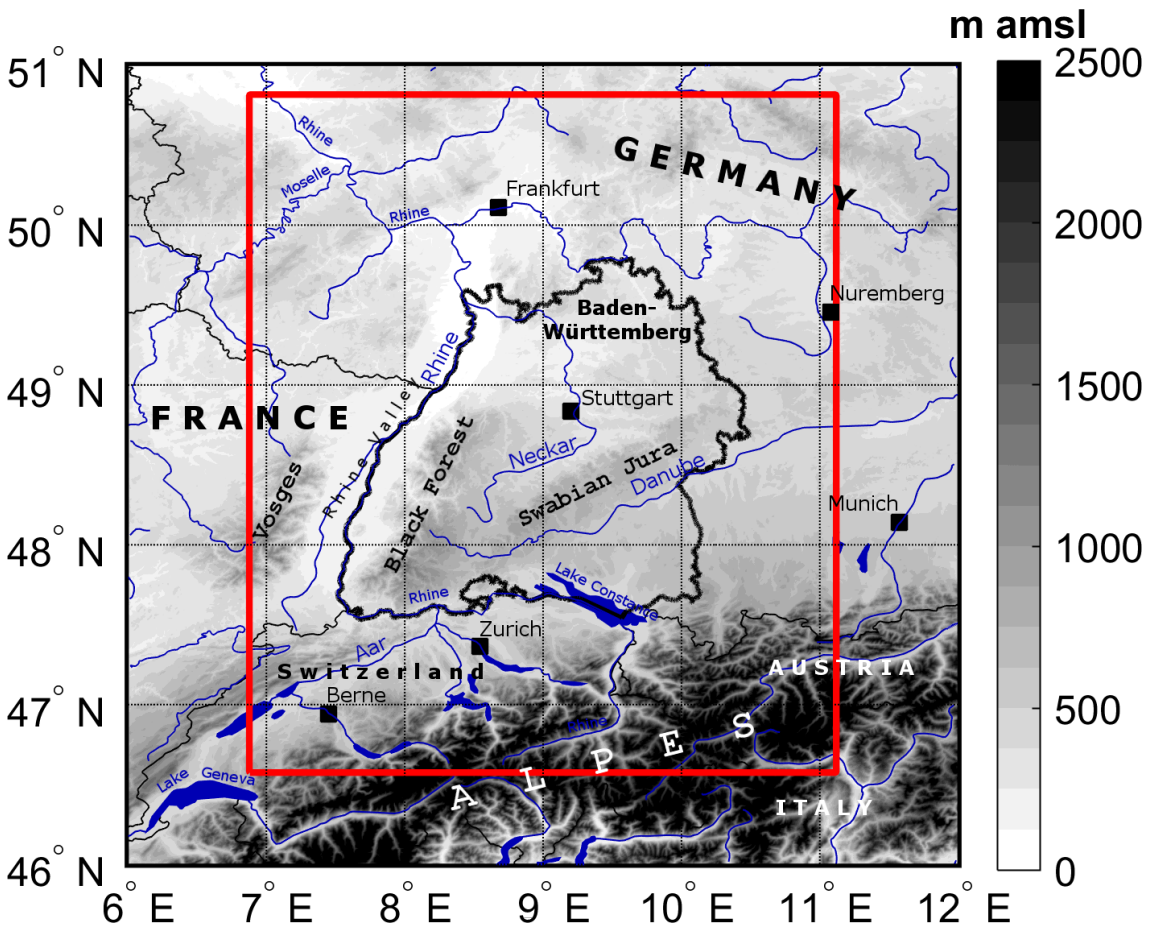

Figure 1. Topographic map of Southwestern Germany and surrounding areas with main river networks and lakes as well as substantial orographic structures; The national borders (slim solid black contours) and the border of the Federal State of Baden-Württemberg (bold solid black contour) are shown as well as the model domain (red box).

northeast. Annual precipitation is between 600 mm (southern Rhine Valley) and approximately 2000 mm (southern Black Forest).

The presented SPM2D is one component of a risk assessment methodology that estimates the risk for a local direct insurer by quantifying the maximum probable loss for a 200-year return period (PML200). The other risk assessment components, however, are not further discussed in this paper.

The paper is structured as follows: Section 2 introduces the basics of the SPM2D. Section 3 briefly describes the data sets used in this study. Section 4 presents the results of the calibration based on a set of 200 historical heavy rainfall events and gives a sensitivity study of the model depending on varying ambient conditions. Section 5 shows some characteristics of the selected events. Results of the stochastic simulations are discussed in Section 6, and Section 7 lists some conclusions.

2 Stochastic Precipitation Model

2.1 General description

The SPM2D, designed for widespread precipitation from essentially stratiform clouds, quantifies total precipitation R_{tot} from the linear superposition of four processes and terms:

$$R_{\mathrm{tot}} = R_{\mathrm{oro}} + R_{\infty} + R_{\mathrm{front}} + R_{\mathrm{conv}} \,. \tag{1}$$

R_{oro} estimates orographic rain enhancement, representing the central core of the SPM2D for complex terrain, as for instance those in BW. R_{∞} is the background precipitation related to large-scale lifting. These two parts originate from the linear orographic precipitation model of Smith and Barstad (2004) and Barstad and Smith (2005) with a few modifications, hereinafter referred to as reduced SPM2D (rSPM). In an extension of the rSPM, we included two additional precipitation components: R_{front} to account for precipitation related to synoptic fronts, and R_{conv} to consider embedded convection atop mainly stratiform clouds (e.g., Fuhrer and Schär, 2005; Kirshbaum and Smith, 2008). These two components were included because the related processes significantly contribute to the total precipitation amount and linear theory, at the same time, tends to an underestimation of low intensities (e.g., Kunz, 2011).

The SPM2D is an event-based model. Instead of simulating continuous long-term periods of several years, a specific number n_{E} of independent events with various duration t_{ev} occurring during different seasons is simulated. The individual components are discussed more detailed in the following Sections. Starting the iteration loop over n_{E} events, first, the characteristics season and duration t_{ev} are allocated to the event (Fig. 2). Next step is the computation of the precipitation fields within the loop over t_{ev}. The components of the total precipitation in Eq. (1) are separated into two types: R_{oro} and R_{∞} are simulated 12-hourly (2 times a day), while R_{front} and R_{conv} are calculated 24-hourly (once a day). The linkage between the precipitation components and the corresponding input variables (pdfs; parameters) is also shown in Fig. 2. Note that the internal free model parameters are set to constant values for the entire simulation (illustrated as shaded box). After each 24-hour period, the total precipitation R_{tot} sums up according Eq. (1). In case t_{ev} is reached, the computation goes on to the next event until n_{E} events have been simulated.

Since the purpose of the model is to stochastically simulate a large number of several thousands events, the results can be used to robustly estimate rare events, such as the one-in-200-year events that the insurance industry must consider (probable maximum loss, PML200). The prerequisite, however, is a decent simulation of single events.

2.2 Orographic precipitation

The linear precipitation model of Smith and Barstad (2004) and Barstad and Smith (2005), which is briefly described in this subsection, is a simple yet efficient way to compute precipitation over complex terrain. A total number of only seven atmospheric parameters estimated from sounding data (see Sect. 3.2) is required to run the model. It is based on the three-dimensional (3D) linear flow according to Smith (1980) and Smith (1989). Thus, it explicitly considers linear flow effects evolving over mountains, such as upstream-tilted gravity waves or flow that goes around rather than over an obstacle in the

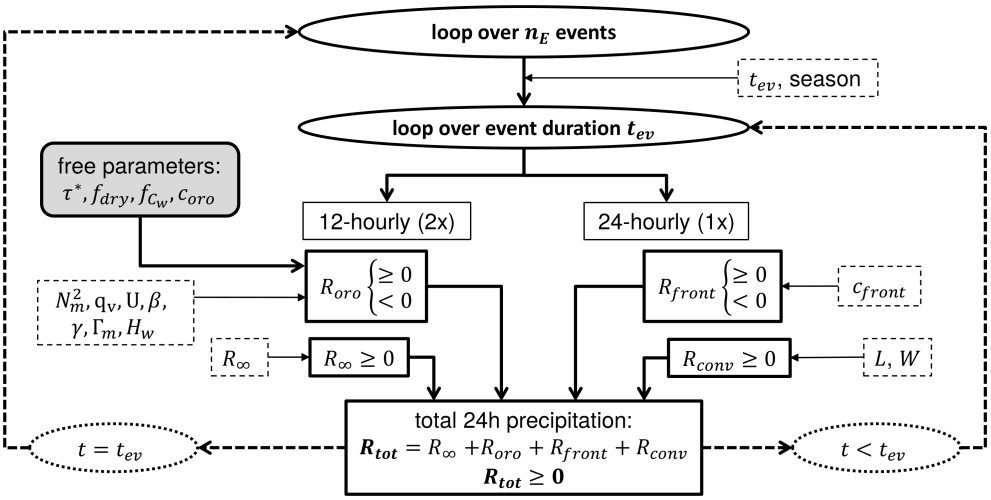

Figure 2. Flow chart of the individual components within the SPM2D (solid boxes) and the corresponding input variables (pdfs; dashed boxes). Iteration loops are highlighted as ellipsis or bold dashed arrows. The constant model parameters are illustrated as shaded box.

case of low wind speed, high static stability, and/or large mountains (i. e. small Froude numbers). It is assumed that saturated lifting produces condensed water that falls to the ground after a certain time shift (Jiang and Smith, 2003). Thus, precipitation on the ground is directly related to the condensation rate.

One of the key components of the linear model is a pair of linear steady-state equations for the advection of vertically integrated cloud water and hydrometeor density, q_c and q_h, during characteristic time scales:

$$\mathbf{v} \cdot \nabla q_\mathrm{c} = S(x,y) - \frac{q_\mathrm{c}}{\tau_\mathrm{c}}\,, \tag{2}$$

$$\mathbf{v} \cdot \nabla q_\mathrm{h} = \frac{q_\mathrm{c}}{\tau_\mathrm{c}} - \frac{q_\mathrm{h}}{\tau_\mathrm{f}}\,, \tag{3}$$

where τ_c and τ_f are time scales for cloud water conversion and the fallout of hydrometeors respectively. Both time scales are mathematically analogous and are assumed to be constant in time and space. When the time scales are set to zero, the maximum precipitation is almost one order of magnitude larger compared with a configuration with, for example, $\tau_\mathrm{f} = \tau_\mathrm{c} = 1000$ s (Kunz, 2011). The source term S describes the mass flux of precipitation caused by orographic lifting. For positive S, $q_\mathrm{c}\tau_\mathrm{c}^{-1}$ acts as a source in Eq. (3) and as a sink in Eq. (2). This term is proportional to the cloud water density integrated vertically from the bottom to the top of the lifting area. In light of this fact, it is assumed that the whole column is saturated in the case of lifting. The loss of hydrometeors, $q_\mathrm{h}\tau_\mathrm{f}^{-1}$ in Eq. (3) is proportional to the hydrometeor column density and determines the precipitation rate R. However, in the case of descending air with negative S downstream of mountains, evaporation occurs, and R may become negative.

A powerful method for the solution of the advection equations for cloud physics, Eq. (2) and (3), together with the linear theory for 3D flow is to apply a two-dimensional (2D) Fourier transform. In Fourier space, the precipitation rate $\hat{R}(k,l)$ is

given by the following transfer function:

$$\hat{R}(k,l) = \frac{iC_{\mathrm{w}}\sigma\hat{h}(k,l)}{(1-imH_{\mathrm{w}})(1+i\sigma\tau_{\mathrm{c}})(1+i\sigma\tau_{\mathrm{f}})}\,, \tag{4}$$

which connects the precipitation field in Fourier space, $\hat{R}(k,l)$, to the orography, $\hat{h}(k,l)$, both related to the horizontal wavenumbers (k,l). In Eq. (4), i is the imaginary unit, and $C_{\mathrm{w}} = \rho_{\mathrm{S_{ref}}}\Gamma_{\mathrm{m}}\gamma^{-1}$ is the uplift sensitivity related to condensation rate $\rho_{\mathrm{S_{ref}}} = \rho_{\mathrm{d}}q_{\mathrm{v}}$, where ρ_{d} is the density of dry air, q_{v} the water vapor density, and Γ_{m} and γ are the moist adiabatic and actual lapse rates respectively. Water vapor scale height H_{w} is the height above ground where the vertical integrated horizontal water vapor flux has reached e^{-1} of its ground value. $\sigma = Uk + Vl$ is defined as the intrinsic frequency with components U and V of the undisturbed horizontal wind vector that is assumed to be constant through time and space.

Whereas the nominator of Eq. (4) gives the dependency of precipitation on vertical motion and orography, the first bracket of the denominator describes the relation of the source term to airflow dynamics. The second and third terms of the denominator consider the advection of hydrometeors during characteristic time scales τ_{x} $(x = c; f)$ and evaporation in the case of descent.

Vertical wavenumber m in Eq. (4) is given by the dispersion relation (Smith, 1980):

$$m(k,l) = \left[\frac{N_{\mathrm{m}}^2 - \sigma^2}{\sigma^2}(k^2+l^2)\right]^{0.5}. \tag{5}$$

In this formulation, m controls both the depth and tilt of forced ascent or descent. Because vertical lifting is assumed to be saturated throughout the whole column, meaning that the lifted condensation level is located at the ground, saturated Brunt-Väisälä frequency N_{m} has to be considered instead of the dry one, N_{d}. Compared with unsaturated flow, saturated flow leads to a weakening of the amplitude of gravity waves via the reduction of static stability and thus to a flow streaming more directly over the mountains rather than around as shown, for example, by Durran and Klemp (1982) or Kunz and Wassermann (2011). Even though the concept of saturated flow by simply considering N_{m} must be regarded as an approximation of the reality, it has been successfully applied by several authors studying flow dynamics and precipitation (Jiang and Smith, 2003; Smith and Barstad, 2004; Kunz and Wassermann, 2011).

The precipitation field on the ground is obtained via an inverse Fourier transform of the transfer function Eq. (4):

$$R_{\mathrm{oro}}(x,y) = \iint \hat{R}(k,l)\mathrm{e}^{i(kx+ly)}\mathrm{d}k\mathrm{d}l\,. \tag{6}$$

Note that R_{oro} can attain negative values meaning a reduction of precipitation totals of superimposed processes. Even though $R_{\mathrm{oro}} < 0$ might be mathematically possible, a negative total precipitation does not make sense physically and thus is truncated away. Therefore, we set $R_{\mathrm{tot}}(x,y) = \max(R_{\mathrm{tot}}(x,y),0)$ at the end of the summation in (1).

The model has five internal free parameters that can be used to adjust/calibrate the model to the observations. Three of these parameters are implicitly considered in the transfer function (Eq. 4): the two time scales of τ_{c} and τ_{f}, which, however, are virtually identical, and the uplift sensitivity factor C_{w}. The latter is modified with a multiplier to $C_{\mathrm{w}}^{*} = f_{\mathrm{C_w}} \cdot C_{\mathrm{w}}$ with the new factor C_{w}^{*} replacing the original C_{w} in Eq. (4). $f_{\mathrm{C_w}}$ reduces the sensitivity of the model for lifting, and therefore, the precipitation rate is reduced, especially over mountainous terrain with sharp gradients, whereas in regions with less orographic

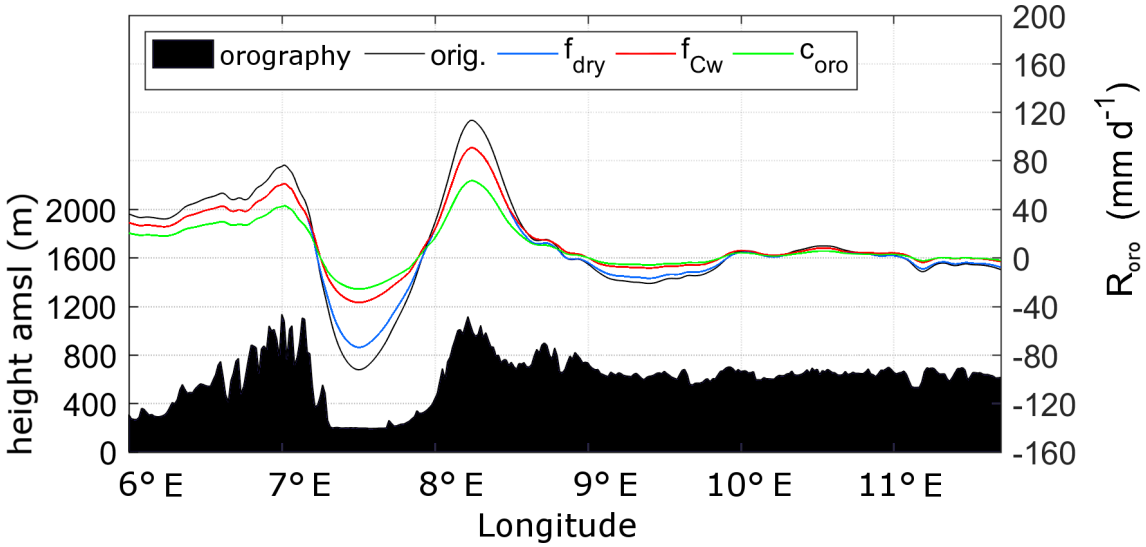

Figure 3. Different effects of the implemented internal free parameters f_{dry} (blue), $f_{\mathrm{C_w}}$ (red) and c_{oro} (green) on the original orographic precipitation part (black curve) for a west to east cross section through the model domain. The underlying orography is shown in black.

gradients the effect is weak (Fig. 3, red curve). The used model formulation also allows for multiple ascents/descents of a virtual air parcel without any change in its water vapor content. Actually, water vapor is partly removed due to condensation processes during ascent, which is realized by $f_{\mathrm{C_w}}$.

An additional parameter, f_{dry}, is implemented in Eq. (6) to reduce evaporation in descent regions, where R_{oro} is negative (Fig. 3, blue curve). The resulting underestimation of precipitation is found especially downstream of steeper mountains with greater descent (Kunz, 2011). Parameter f_{dry} acts only at grid points (x, y) where $R_{\mathrm{oro}} < 0$, in which $f_{\mathrm{dry}} < 1$; in all other cases $f_{\mathrm{dry}} = 1$.

Finally, the last additional calibration parameter, c_{oro}, reduces orographic precipitation in the whole domain (Fig. 3, green curve). It is a consequence of the assumption that the vertical lifting of an entire air column with saturation produces condensate and instantaneous fallout at any time, implying an overestimation of precipitable water. In reality, not all layers are completely saturated, and water may also partly be stored by clouds. Parameter c_{oro} is implemented similarly to f_{dry} in Eq. (6) but is independent of any lifting processes and constant for the whole domain. With these two parameters, orographic precipitation is modified to:

$$R^{*}_{\mathrm{oro}}(x, y) = f_{\mathrm{dry}} \cdot c_{\mathrm{oro}} \cdot R_{\mathrm{oro}}. \tag{7}$$

Note again that f_{dry} affects only grid points with net descent, whereas c_{oro} is constant over the whole domain. From a mathematical perspective the two factors $f_{\mathrm{C_w}}$ and c_{oro} could collapse to one single parameter. Nevertheless, they describe modifications on different physical processes as mentioned in the section above and, hence, have to remain separate.

2.3 Background precipitation

The background precipitation term R_∞ in Eq. (1) describes the effect of large-scale lifting by synoptic-scale weather patterns. According to the ω-equation, lifting is the result of three different mechanisms: positive vorticity advection increasing with height (or vice versa); the maximum of diabatic phase transitions; and the maximum of warm air advection. Even though lifting is the superposition of these three mechanisms, we do not split R_∞ accordingly, as the single forcing terms can not be estimated out of radiosounding data. Furthermore, we assume that the large-scale conditions are almost horizontally homogeneous across the investigation area, and so is R_∞ at each time step.

To simplify the inclusion of large-scale lifting in the SPM2D, we estimate R_∞ from observed rainfall totals (see Sect. 3.1) over a larger area with almost flat terrain, where R_{oro} as well as evaporation by ascent are minimized to a large degree. However, an analysis of various past events shows the strong variability of the spatial distribution of precipitation even over flat terrain. For example, some events affect only the northern parts of the investigation area, whereas other occur only in the southern parts. To ensure a proper estimation of R_∞, we choose an area that covers most of the total investigation area but excludes the Black Forest and prealpine lands. In the region, where we estimate R_∞ (Fig. 4, black box), heavy rainfall is very unlikely. Totals of more than 50 mm per day, for example, exhibit an annual exceedance probability p of less than 0.5. Furthermore, as confirmed by Fig. 4, the probability of rain totals in excess of 50 mm per day is more or less homogeneously distributed. On average over 66 years, it can be assumed that precipitation in the area used for R_∞ estimation mainly results from large-scale lifting and to a lesser extent from orographic influences.

2.4 Frontal precipitation

Apart from large-scale lifting connected to low-pressure systems or waves in the flow patterns, precipitation is also substantially enhanced by weather fronts. Active fronts may increase precipitation considerably due to cross-frontal circulations and lifting in the warm sector of a cyclone (e. g., Bergeron, 1937; Eliassen, 1962). Conversely, if a front affects only parts of the investigation area (e.g., a trailing front, where the flow is almost parallel to the frontal alignment), regions outside the sphere of influence may experience much less or even no rain at all. Both effects are considered by implementing an additional quantity R_{front} in Eq. (1):

$$R_{\mathrm{front}} = (R_{\mathrm{oro}} + R_\infty) \cdot (c_{\mathrm{front}} - 1)\,, \tag{8}$$

where c_{front} serves as the enhancement or reduction factor of the overall precipitation. In this simple parameterization, R_{oro} is considered again because frontal precipitation is additionally enhanced by orography as shown, for example, by Browning et al. (1975) or Houze and Hobbs (1982). Due to the additive superposition of all precipitation components in Eq. (1), we have to subtract the original precipitation totals leading to a total multiplier $(c_{\mathrm{front}} - 1)$. The frontal enhancement factor is a function of space realized by a rectangular area $c_{\mathrm{front}}(x, y)$, where the orientation of the y-axis is prescribed by the mean wind direction β (Fig. 5).

To avoid strong gradients at the border areas of the rectangular, we applied Gaussian-shaped smoothing. Along the x-dimension, the spread is set to $8\sigma_{\mathrm{n}}$, where σ_{n} is the standard derivation of the normal distribution. In the y-direction, an

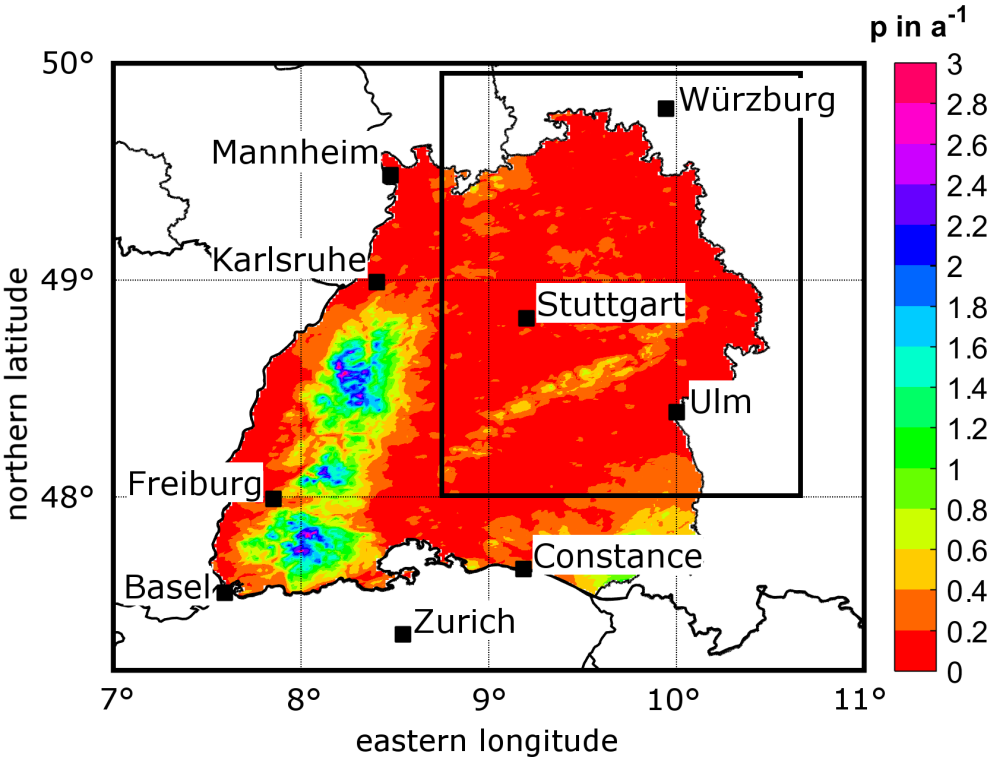

Figure 4. Probability of observed 24-hour rainfall totals greater than 50 mm expressed as the average days per year for Baden-Württemberg; the black box indicates the area, where background precipitation R_∞ is estimated.

infinitesimal length is considered (Fig. 5). As the minimum of c_{front} is zero, R_{front} can also attain negative values, thus leading to a weakening of total precipitation in an area affected or not affected by a front. In order to calculate c_{front} from the observational data, we define this quantity as the relative difference between observations O and output M of the rSPM (neglecting embedded convection as described in the next paragraph). This is expressed by

$$c_{\mathrm{front}} = \overline{O} \cdot \overline{M}^{-1} \tag{9}$$

assuming that the differences originate primarily from frontal effects. For the quantification of c_{front}, we use spatial mean values over the investigation area $\overline{O}$ and $\overline{M}$ for a training sample of historic heavy precipitation events (see Sect. 2.6).

2.5 Embedded Convection

The last part of the total precipitation model SPM2D considers convection embedded in mainly stratiform clouds (e. g., Fuhrer and Schär, 2005). Note, however, that the model is not foreseen to simulate purely convection. Such embedded convection mainly occurs when lifting is locally enhanced at mid- and upper tropospheric levels leading to a decrease of thermal stability by the release of the latent heat of condensation (e. g., Kirshbaum and Durran, 2004; Kirshbaum and Smith, 2008; Cannon

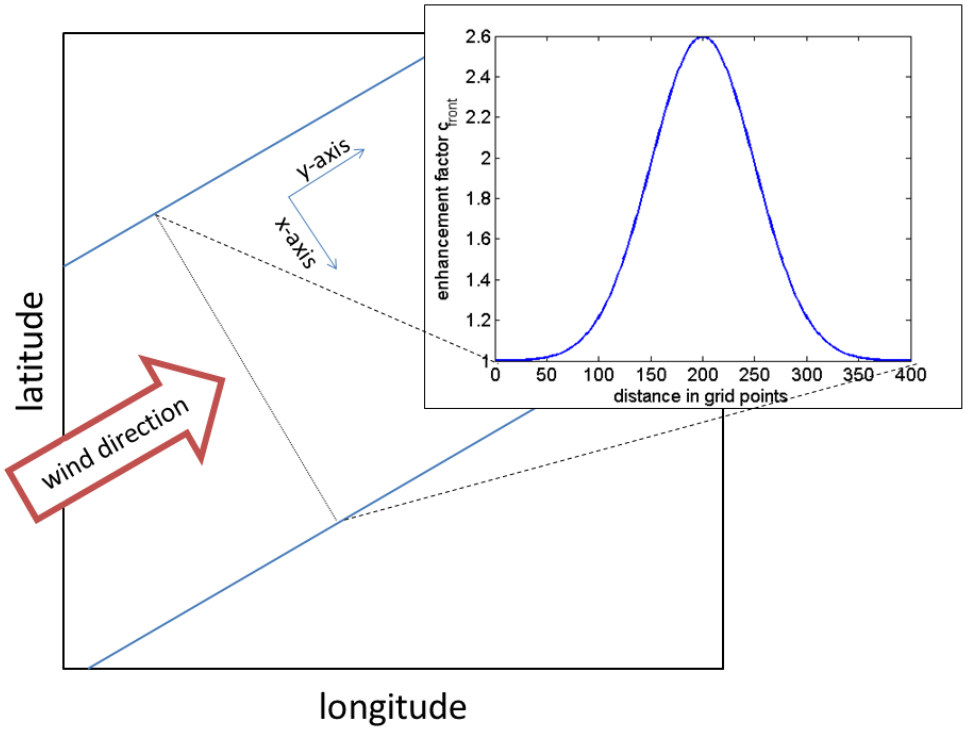

Figure 5. Schematic of a Gaussian-shaped distribution of the frontal enhancement factor with $c_{\mathrm{front}} = 2.6$ and $\sigma_{\mathrm{n}} = 50$ (upper right corner) and its location in the model domain for a southwesterly wind direction (arrow). The blue lines indicate the boundaries of the frontal zone.

et al., 2012). Convection in general involves several complex processes that make simulation a difficult task. Since our model is restricted to large-scale precipitation with the objective of quantifying extremes in terms of areal precipitation solely, we treat embedded convection in a very simplified way by implementing several rectangular cells similar to the approach of frontal system consideration.

Because embedded convection is also partly induced by orographic precipitation mechanisms, we implemented a multiplicative factor to the precipitation fields related to both orographic and large-scale lifting, similar to the frontal part:

$$R_{\mathrm{conv}} = c_{\mathrm{conv}} \cdot (R_{\mathrm{oro}} + R_{\infty}), \tag{10}$$

with enhancement factor c_{conv}.

For each time step of the simulation, we choose a number of convective cells, each with specific width W and length L, and distribute them randomly over the whole model domain (Fig. 6). Both width W and length L of each rectangle of the convective cells are estimated from the characteristics of the severe convective storms identified from radar data by Fluck, 2018 (see Sect. 3.3). Furthermore, we restricted the two parameters to $L > W$ and $L_{\max} = 300\,\mathrm{km}$, or 300 grid points, respectively. As for the frontal systems, the wind direction defines the orientation of the longer sides of the rectangles. For each convective

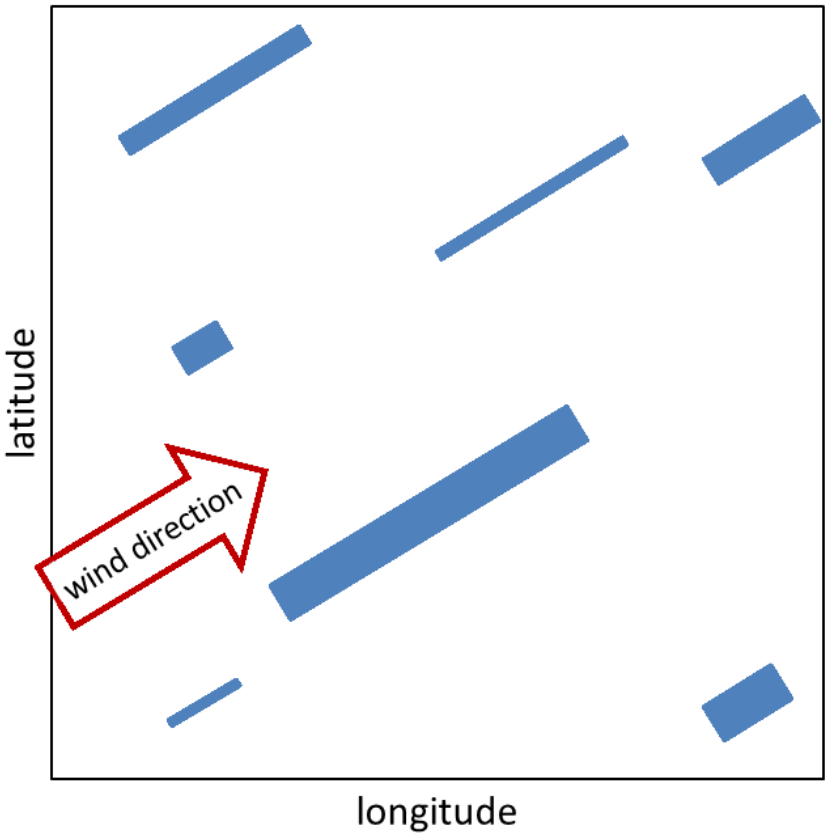

Figure 6. Schematic of the convection implementation with rectangular cells (blue). The orientation is defined by the wind direction (arrow); each cell is assigned to an individual factor c_{conv}.

cell, we choose $L \cdot W$ specific factors c_{conv} with $c_{\mathrm{conv}} \in \{0; 1\}$. As found, for example, by Fuhrer and Schär (2005) or Cannon et al. (2012), embedded convection can enhance precipitation up to 200 %; thus, the given range of c_{conv} is adequate. Within the single cells, the spatial distribution of c_{conv} randomly varies between the given limits. Summing up all cells enables the existence of more than one cell per day at a specific grid point. The complete convective precipitation field for each time step is spatially smoothed to avoid sharp gradients. In contrast to the Gaussian shape smoothing due to a more or less continuous increase/decrease of precipitation enhancement in the case of fronts, we use a moving average with a span of 10 grid points to preserve the high spatial variability of convection.

2.6 Event definition and statistical distribution functions

Stochastic modeling of precipitation events with SPM2D requires the adjustment of appropriate probability density functions (pdfs) to all input parameters. These pdfs are estimated from an adequate set of past heavy rainfall events. Based on the pdfs,

several thousands events can be stochastically generated. Because the characteristics of the ambient conditions and thus the precipitation regimes change throughout the year, we seasonally differentiate the estimated pdfs among spring (MAM), summer (JJA), autumn (SON), and winter (DJF).

In the first step, a sufficient and appropriate subset of relevant historic events has been identified. An event here is defined as a period of one or more days with persisting precipitation above a certain threshold of daily precipitation. Because our study focuses on major large-scale flood events and not on local-scale floods or flash floods, an extension to multi-day events is reasonable to consider time delays in discharge response or flood waves traveling along river networks (e. g., Duckstein et al., 1993; Uhlemann et al., 2010; Schröter et al., 2015).

We define the historic event set based on maximum areal precipitation. For this, we simply accumulate the (equidistant) 24-hour rainfall totals $\overline{R}_{\mathrm{BW}}$ of all grid points in BW (see Sect. 3.1). Following the sorting of all values of $\overline{R}_{\mathrm{BW}}$ in descending order, the strongest 200 values enter the sample (top200). As precipitation is not limited to these (single) days but may be embedded in longer time periods, we define the threshold R_{thres} for event definition. Estimating R_{thres}, we consider "wet" days by using $\overline{R}_{\mathrm{BW}} > 0$ solely, and set R_{thres} to the 75 % percentile of this sub-sample. A lower threshold leads to an over-interpretation of longer clusters, a higher one avoids multi-day events.

Event precipitation starts on the first day that exceeds R_{thres}. When areal means of consecutive days are also above R_{thres}, they are simply accumulated, yielding events of more than one day. The last day with $R \geq R_{\mathrm{thres}}$ before a period of at least three days of non-exceedance defines the end of an event. Such a three-day period ensures statistical independence of the events in accordance with the approach of Palutikov et al. (1999) for wind storms. Following Piper et al. (2016), we only count "rain days" ($\overline{R}_{\mathrm{BW}} \geq R_{\mathrm{thres}}$) and neglect "skip days" ($\overline{R}_{\mathrm{BW}} < R_{\mathrm{thres}}$) in between the start-day/end-day period for event duration estimation, which is a widely used approach (Wanner et al., 1997; Petrow et al., 2009). This approach avoids the over-interpretation of longer clusters.

Based on the procedure described above, a defined precipitation event contains one or more days of the top200 sample. For this event set, all required input parameters were extracted from sounding data and rainfall totals (see Sect. 3).

In the next step, we identified the pdfs most appropriate for statistically describing each of the seven atmospheric input parameters, event duration t_{ev}, background precipitation R_{∞} and front factor c_{front}. In addition to 20 pdfs preset by the MATLAB statistic toolbox (MATLAB, 2016), we considered the circular von-Mises distribution (Mardia and Zemroch, 1975) for wind direction only. In total, 17 pdfs were suitable, and tested and compared with the distribution of each parameter for each of the four seasons (Table 1). Note that Gumbel (GbD) and Weibull (WbD) distributions are special cases of the generalized extreme value distribution (GEV) and that some pdfs cannot be used for every parameter due to their ranges of validity.

To find the pdf that best fits the data, we estimated the appropriate number of histogram classes according to Freedman and Diaconis (1981), and we calculated the bias, root mean square error (rmse) and Spearman correlation coefficient r_{Sp} (Spearman, 1904) as quality indicators (QIs). We also applied a χ^2-test according to Wilks (2006) as a QI. For each QI, we ranked the pdfs in ascending order and added up the rank numbers for each pdf receiving the best fit in terms of the least QI–rank sum (QIRS). In the case of alikeness of two or more pdfs (about 10 % of all cases), we manually selected the best one.

3 Data sets

The SPM2D presented in this study is based on two different types of data sets: gridded precipitation data to estimate background precipitation and to calibrate and verify the model, and vertical profiles from radiosondes to initialize the model. Furthermore, the SPM2D is also validated with reanalysis data done with the regional climate model of the Consortium for Small Scale Modeling (COSMO-CLM). Unless otherwise indicated, the investigation period covers the years of 1951–2016 (hereinafter referred to as IP).

3.1 Rainfall totals

Rainfall statistics in our study are based on the REGNIE (German: ***REG****ionalisierte* ***NIE****derschläge*; regionalized precipitation) data set provided by the German Weather Service (Deutscher Wetterdienst; DWD). REGNIE is a gridded data set of 24-hour totals based on several thousand climate stations more or less evenly distributed across Germany (so-called RR collective). The REGNIE algorithm interpolates the observations to a regular grid of approximately 1 km^2 considering elevation, exposition, and climatology (Rauthe et al., 2013). The REGNIE domain covers the area with $5.83^\circ\,\mathrm{E} \leq \phi \leq 16^\circ\,\mathrm{E}$ and $47^\circ\,\mathrm{N} \leq \theta \leq 55.08^\circ\,\mathrm{N}$ (ϕ: longitude; θ: latitude). Grid points outside of Germany are set to a missing value. The observation period is from 06 to 06 UTC.

It should be noted that REGNIE data are temporally not homogeneous due to changes in the locations and number of rain gauges. Furthermore, areal precipitation exhibits a certain bias especially over elevated terrain, such as the Black Forest mountains, because the number of stations considered by the regionalization is limited. Its magnitude, however, cannot be directly estimated from the observations (Kunz, 2011).

We use the REGNIE data set for the definition of the top200 data set, event duration, background precipitation and the front factor c_{front}, and for the validation of the SPM2D.

Table 1. List of the tested and suitable pdfs preset in the MATLAB statistical toolbox (the short acronyms in brackets are for further orientation).

Birnbaum-Saunders (BSD)	Nakagami (NkD)
Gamma (GmD)	Normal (ND)
Generalized Extreme Value (GEV)	Poisson (PD)
Gumbel (GbD)	Rayleigh (RyD)
Half-Normal (HND)	Rician (RcD)
Inverse Gaussian (IGD)	Stable (SD)
Logistic (LD)	Student's t (StD)
Log-Logistic (LLD)	Weibull (WbD)
Log-Normal (LND)	

3.2 Radiosoundings

Input of the SPM2D are seven atmospheric parameters derived from radiosoundings: thermal stability in terms of saturated Brunt-Väisälä frequency N_m (e. g., Lalas and Einaudi, 1973) and actual and saturated vertical temperature gradients (γ and Γ_m), water vapor scaling height H_w, water vapor mixing ratio q_v, wind speed U, and direction β (see Sect. 2). These parameters are computed from the vertical profiles of temperature, moisture, wind speed, and direction at the radiosounding station of Stuttgart (48.83° N 9.20° E) located somewhat downstream of the northern Black Forest mountains. Even though the location might not be ideal because the profiles do not represent undisturbed conditions, the profiles are similar to that of the upstream station of Nancy in France as shown by Kunz (2011) for heavy rainfall events on average. Data from Nancy, however, are available after 1990 only and, thus, cannot be used in this study, whereas soundings from Stuttgart are available since 1957. We used the soundings at the main standard times for synoptic observations (00 and 12 UTC).

Sounding data were provided by the Integrated Global Radiosonde Archive (IGRA) for quality-controlled radiosonde and pilot balloon observations from the National Climatic Data Center (Durre et al., 2006). These data, available at both main pressure levels and levels of significant changes of one of the parameters, were interpolated into equidistant increments of $\Delta z = 10$ m (Mohr and Kunz, 2013). All parameters derived from the soundings refer to the lowest 5 km of the atmosphere since this layer is most relevant for air flow and stability. Furthermore, to account for the decreasing impact of higher atmospheric layers on the flow characteristics, all flow parameters Λ have been vertically integrated ($\widetilde{\Lambda}$), with a water vapor weighting being applied (Kunz, 2011):

$$\widetilde{\Lambda} = \frac{\int_{z=0}^{z_\mathrm{t}} \Lambda \rho_\mathrm{d} q_\mathrm{v}\, dz}{\int_{z=0}^{z_\mathrm{t}} \rho_\mathrm{d} q_\mathrm{v}\, dz}, \tag{11}$$

where ρ_d is the density of dry air and $z_\mathrm{t} = 5000$ m.

As some layers may be moist-unstable, resulting in imaginary N_m, the averaging routine is applied to N_m^2. In the few cases where $\widetilde{N}_\mathrm{m}$ was imaginary, it was set to a near-neutral, constant value of 0.0003 s^{-1}.

3.3 Parameters for Embedded Convection

Embedded convection in the SPM2D is considered by single streaks of enhanced precipitation (see Sect. 2.5). These streaks are stochastically generated according to the statistical distributions of the observed maximum length L and width W of severe convective storms estimated by Fluck (2018). In that study, convective storms were identified from the constant altitude plan position indicator (CAPPI) for a reflectivity in excess of 55 dBZ, also known as the Mason (1971) criterion for hail detection. The application of a tracking algorithm based on the concept of the algorithm of TRACE3D (Handwerker, 2002) yields entire tracks of convective storms. In total, more than 20,000 tracks over Germany, France, Belgium, and Luxembourg were identified during the summer half years (April to September) in the period 2004–2014. Even though we do not consider rainfall related to severe convective storms or hail in the SPM2D, the statistical distributions of the storm's dimensions are reliable proxies for the extension of enhanced precipitation from embedded convection described by R_conv.

3.4 Numerical Weather Simulations

Simulation results from the SPM2D are validated with rain totals from the non-hydrostatic Consortium for Small-scale Modeling (COSMO) model in climate mode (CCLM; Rockel et al., 2008). CCLM is run by global ERA-40 reanalysis from the European Center for Medium-Range Weather Forecasts (ECMWF) with a resolution of T159, which corresponds to approximately 125 km on 60 vertical layers (Kållberg et al., 2004). The ERA-40 is available for the period from September 1957 to August 2002 and includes the assimilation of several observational data sets such as satellite data. Laube (2018) performed a dynamical downscaling of ERA-40 to a horizontal resolution of 2.8 km for Southern Germany using a threefold regional nesting (50, 7, to 2.8 km). High-resolution CCLM data is available for the period 1971–2000. For the evaluation, we considered the top200 REGNIE events, from which around 100 events occurred within the period where CCLM data are available including the top two and 7 (14) of the strongest 10 (20) events.

4 Calibration

This section describes the calibration of the SPM2D by comparing modeled and observed precipitation fields (REGNIE 24-hour totals). The outcome is a combination of the free parameters with the highest skill of the simulated historic rainfall totals (training sample), which then is used for the stochastic simulations of 10,000 rainfall events (validation sample). The latter is equivalent to a period of several thousand years as described in Sect. 6. At the end of this section a concise study on model sensitivities is given.

4.1 Method

Based on the event set of top200, the free model (calibration) parameters, τ^*, $f_{\mathrm{C_w}}$, f_{dry} and c_{oro}, are assessed. All other parameters required by the SPM2D (cf. Sect. 2) are quantified from radiosounding profiles at Stuttgart. In this evaluation, the stochastic components of the SPM2D and the randomly modeled components for fronts (R_{front}) and embedded convection (R_{conv}) are neglected. Without these components, the model is referred to as the reduced SPM2D (rSPM).

In order to determine appropriate values of the free parameters, a large number of model simulations was carried out with the rSPM. Whereas one parameter was successively varied, the others were kept constant. The selected ranges and increments of the parameters listed in Table 2 resulted in 2,016 possible parameter combinations, giving a total number of approximately 390,000 simulation days for the top200 event set. For each day and parameter combination, we assess the model skill by quantifying both bias and rmse. Both data sets (model output and REGNIE) are slightly smoothed using a running 5×5 grid box. The reason for the smoothing is that REGNIE data, despite having a high resolution of 1 km, exhibit spatial uncertainty due to the limited number of observational data considered. Especially around the crests of Black Forest, where the number of stations is very low, REGNIE data cannot reproduce local peak rainfall totals. Furthermore, as shown, for example, by Barstad and Smith (2005), smoothed data yield more robust results when comparing model and observation data. Note, however, that

larger values of τ^* and smaller values of $f_{\mathrm{C_w}}$, respectively, likewise smooth the simulated precipitation fields. In these cases, the QIRS method used for the evaluation (Sect. 2.6) has to be applied carefully.

To avoid apparently better representations of smoothed data fields, we use skill score S (Eq. 12) described by Taylor (2001) for evaluating climate models to determine the best parameter combination of rSPM:

$$S = \frac{4\,(1+r)}{\left(\hat{\sigma}_f + \frac{1}{\hat{\sigma}_f}\right)^2 \cdot (1+r_0)}\,, \tag{12}$$

where r is the correlation coefficient after Spearman (1904), r_0 the maximum attainable correlation, and $\hat{\sigma}_f = \sigma_{\mathrm{mod}} \cdot \sigma_{\mathrm{obs}}^{-1}$ the normalized standard deviation with the standard deviations of model output σ_{mod} and observations σ_{obs}. For $\hat{\sigma}_f \to 1$ and for $r \to r_0$, S approaches unity, which is the best result. According to Taylor (2001), improved values of rmse or bias do not lead to an actual improvement of the model performance, and the use of correlation and standard deviation is more stable. Furthermore, Taylor (2001) provided no regulation for the estimation of r_0. Therefore, we set r_0 to the maximum calculated correlation coefficient of all simulations. As it is not guaranteed that this maximum is the actual maximum attainable correlation, we increase r_0 by 10 %, yielding $r_0 = 0.93$.

Skill score S is computed for each simulation day and each parameter combination. From all realizations, we select the parameter combination that yields the highest median value of S averaged over all top200 events, as the SPM2D should be able to properly represent a broad range of different atmospheric conditions.

4.2 Calibration Results

Applying the method to the top200 events as described above, the highest median skill score of $\mathrm{S} = 0.60$ is obtained for the combination of $\tau^* = 1400$ s, $f_{\mathrm{C_w}} = 1.0$, $f_{\mathrm{dry}} = 0.4$ and $c_{\mathrm{oro}} = 0.8$. For this combination, the median values of the other quality indices are $r_{\mathrm{Sp}} = 0.39$, $\hat{\sigma}_f = 0.98$, bias = 6.30 mm, and rmse = 14.85 mm. The assessed values for the former two model parameters are physically plausible and comparable to other studies with the rSPM (e.g., Barstad and Smith, 2005; Caroletti and Barstad, 2010; Kunz, 2011). The latter two parameters are incorporated exclusively in this study. However, considering the slight overestimation of orographic precipitation enhancement and the strong overestimation of lee-side drying, the two values seem to be physically plausible as well.

Table 2. The minimum and maximum values, and the increments of the time scales τ^*, and multiplicative factors for the uplift sensitivity $f_{\mathrm{C_w}}$, the lee-side drying f_{dry}, and the adjustment of orographic precipitation c_{oro}.

parameter	minimum	maximum	increment
τ^*	800 s	1500 s	100 s
$f_{\mathrm{C_w}}$	0.5	1.0	0.1
f_{dry}	0.4	1.0	0.1
c_{oro}	0.5	1.0	0.1

The sensitivity of skill score S to τ and to the two other parameters, $f_{\mathrm{C_w}}$ and c_{oro} (Fig. 7), shows a dipole structure in both cases with the highest values of S along a counter diagonal. Minor skill scores are obtained with the shortest (longest) time scales in combination with the highest (lowest) uplift sensitivity or highest (lowest) weighting of R_{oro} in Eq. (1). This implies, on the one hand, that for smaller displacements of precipitation from the formation region, orographic precipitation is overestimated by the rSPM and thus has to be reduced. On the other hand, R_{oro} has to increase for wider displacements.

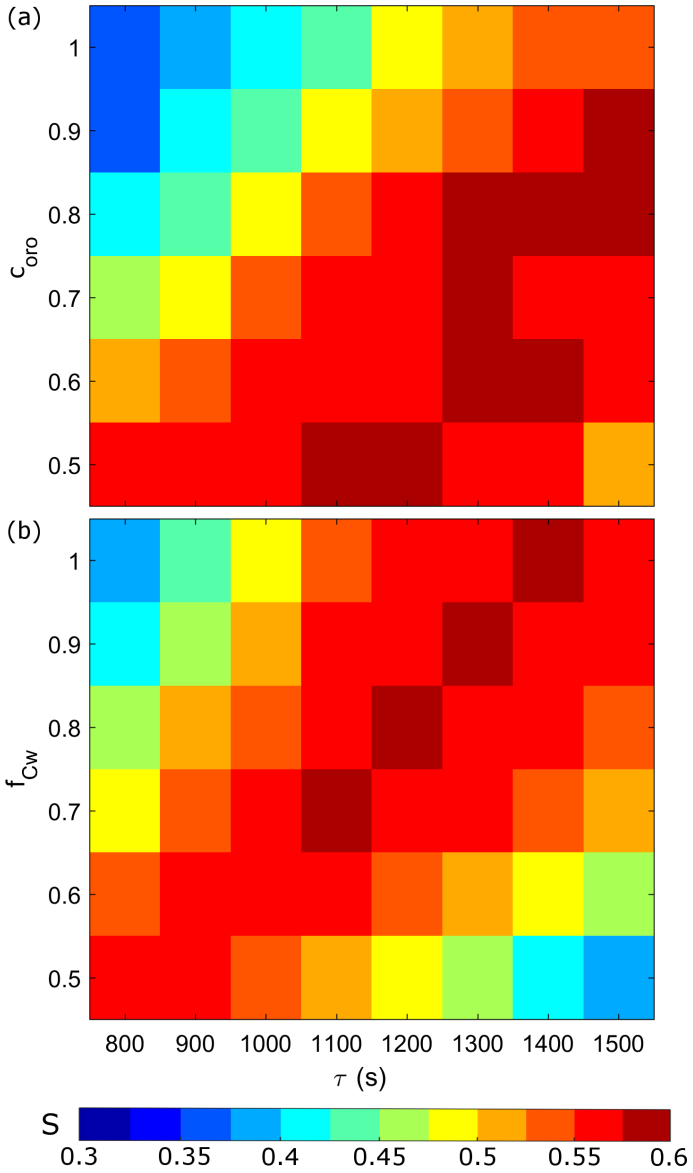

Figure 7. Sill score S, averaged over the top200 event set, depending on τ and (a) c_{oro}, and (b) $f_{\mathrm{C_w}}$, while the other free parameters, respectively, were set to their optimum values.

Note that the above-identified parameter combination yields the lowest errors only when averaging over all events. Single events may become more realistic with another parameter combination, reflecting particularly the unknown, and thus not considered microphysical processes that are decisive for precipitation formation and strongly controlled by vertical wind speed, temperature, and moisture profiles. The dependency of microphysical processes on ambient conditions, however, is not relevant when running the model in the stochastic mode as in this study.

4.3 Sensitivity of simulated total precipitation

To demonstrate how atmospheric conditions translate into precipitation, we conduct a sensitivity study with rSPM using the top200 event set by gradually changing the input parameters. Following Kunz (2011), we perturbed the values of N_{m}^2, q_{v}, U, β, and τ estimated from the top200 events. This is done by multiplying the respective quantity with var_mult increasing linearly from 0.5 to 2.0 in increments of 0.1. Wind direction β is varied in the range of $\pm 30^\circ$ in increments of 5°. The calibration parameters are set to their optimum values estimated in the previous section. Besides areal mean precipitation, we analyze rmse and skill score S for the median over the top200 event set.

Areal mean precipitation accumulated over 24 hours shows a high sensitivity to changes in water vapor content q_{v}, wind speed U and wind direction β (Fig. 8). In all cases, precipitation increases (decreases) with increasing (decreasing) parameter values. Lowest sensitivity occurs for β between $\pm 15^\circ$ because of the orientation of the major orographic structures (e. g., the Black Forest) from southwest to northeast. Westerly inflows, prevailing on average, still occur for small variations of β. For greater shifts ($\Delta\beta > 20^\circ$ or $\Delta\beta < -20^\circ$), when the inflow angle becomes smaller, sensitivity slightly increases. The changes in the wave regimes and, thus, the location of the updraft may also explain the partly stepwise form of the curves for both β and U. The results for varying stability N_{m}^2 and microphysical time scales τ reveal an opposite behavior of areal mean with an increase at smaller values and vice versa. Furthermore, the sensitivity of the model to changes of these two parameters is much weaker compared to the other parameters.

Qualitatively a similar behavior of the model is found for the medians of rmse and skill score S (Fig. 9). While areal precipitation discussed above only provides insights how changes in the ambient parameters feedback into rainfall, rmse and S also consider its spatial distribution. The results for rmse (Fig. 9a) again reveal the highest sensitivity of the rSPM to changes in q_{v} and U. While for $var\_mult > 1$ the sensitivity in terms of rmse is similar to areal precipitation, there is a much higher sensitivity for values below 1. In those cases, orographic precipitation is more detached to the mountain crests resulting in higher totals due to reduced evaporation in the descent regions. Because of the combination of higher totals at different locations, rmse show a higher sensitivity to changes of τ and N_{m}^2 compared to areal mean precipitation.

The skill score S, on the other hand, is most sensitive to changes in q_{v} and τ (Fig. 9b). Regarding N_{m}^2, S decreases just for very high values of var_mult, while there is almost no sensitivity on the wind direction β. In all cases, highest S is obtained for the original values of the input parameters ($var\_mult = 1$ or $\Delta\beta = 0^\circ$), indicating the well calibration of the model.

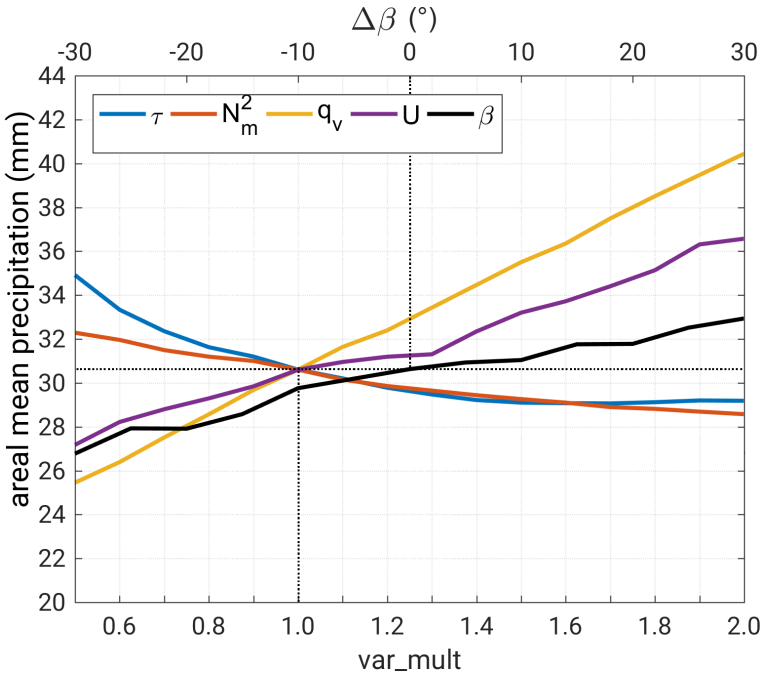

Figure 8. Areal mean precipitation (median of the top200 BW event set) as a function of N_{m}^2, q_{v}, U, β, and τ perturbed by a multiplicative factor ($0.5 \leq var\_mult \leq 2$) and changed $\Delta\beta$. The dotted lines indicate the values of the reference run.

4.4 Case Study

After the parameter adjustment, the rSPM tends to slightly underestimate orographic precipitation, whereas totals over flat or rolling terrain are overestimated. This behavior can be seen, for instance, in the example of 31 May 2013 (Fig. 10), a heavy precipitation event that triggered the severe flooding in 2013 (Schröter et al., 2015).

On that day, a pronounced low pressure system with its center over Croatia led to the sustained advection of moist airmasses from northerly directions around 20° in combination with synoptic-scale ascent. The Stuttgart sounding with low stability ($N_{\mathrm{m}} = 0.0055\,\mathrm{s}^{-1}$), high precipitable water ($pw = 24\,\mathrm{kg\,m}^{-2}$), and high wind speed ($U = 20\,\mathrm{m\,s}^{-1}$), the latter two determining the horizontal water vapor flux, is already an indication of high precipitation totals. Consequently, precipitation totals across the investigation area reached values between 10 and 100 mm.

Overall, the rSPM is able to reproduce most of the structures of the observed rain field (Fig. 10). The quality indices for that day are $S = 0.62$, $r_{\mathrm{Sp}} = 0.30$, $\hat{\sigma}_{\mathrm{f}} = 0.75$, bias = 4.44 mm, and rmse = 14.82 mm. The best agreement between observed and simulated precipitation fields is found for the Northern Black Forest as well as Swabian Jura. Over the northern part of the model domain (north of 49° N) and southwest of Stuttgart, simulated rainfall is substantially higher compared with REGNIE. By contrast, the rSPM simulates lower totals in the Southern Rhine Valley near and over the mountainous regions

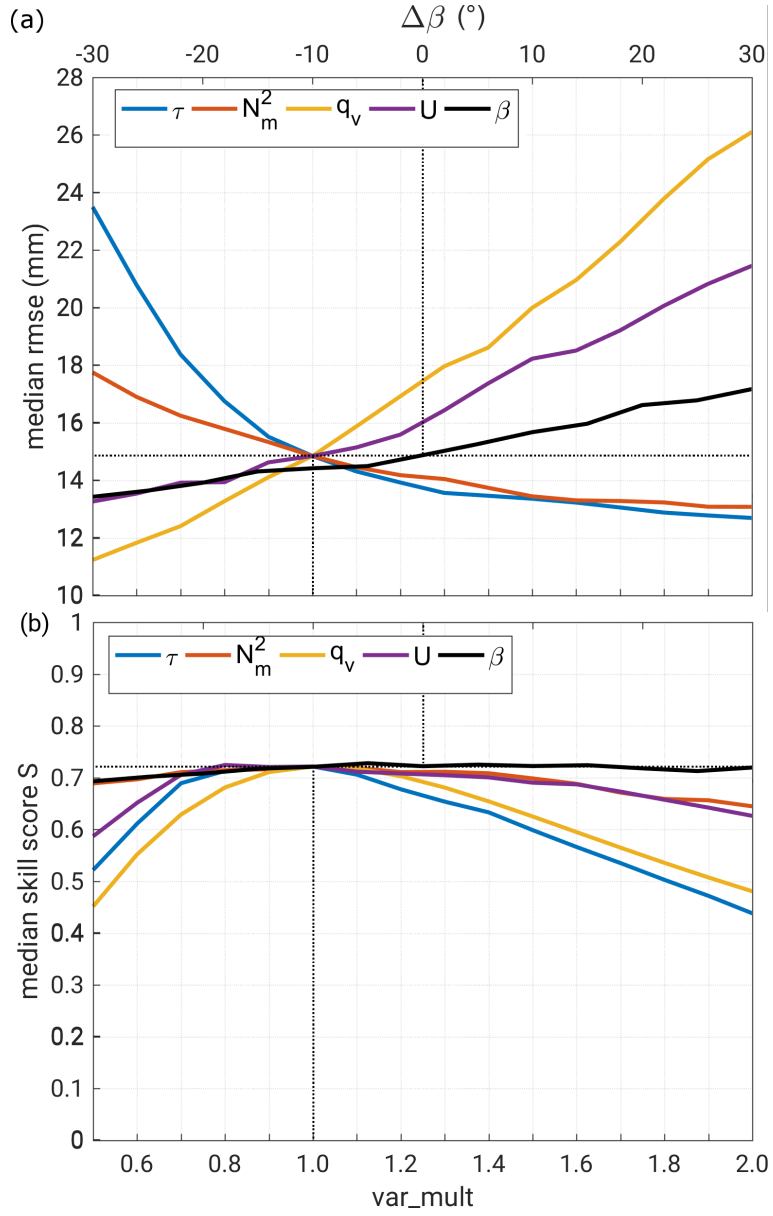

Figure 9. Same as Fig. 8, but for (a) median rmse and (b) median skill score S.

of the Southern Black Forest (around Freiburg), especially east of the Basel region, where lee-side evaporation in the model dominates.

One reason for the discrepancy between observed and simulated precipitation might be the ill-suited location of the Stuttgart sounding used for the model initialization. The sensitivity study as described in Sect. 4.3 for this particular event obtains the

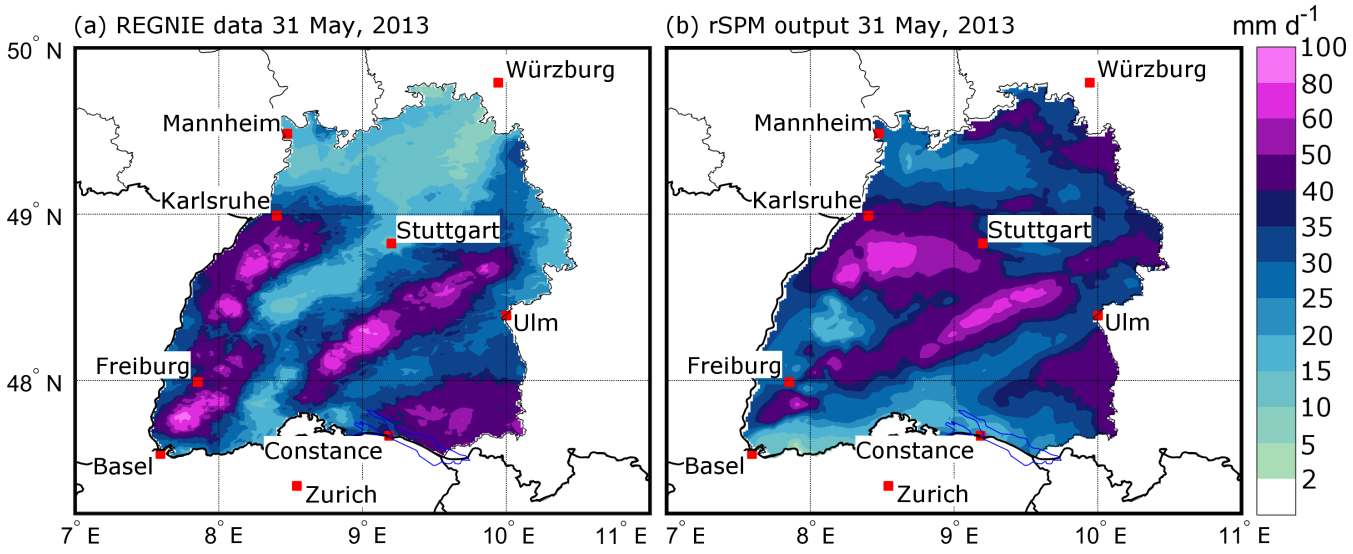

Figure 10. Comparison of (a) REGNIE 24-hour rainfall totals, and (b) rSPM output for Southwest Germany, exemplary on 31 May, 2013. Note that REGNIE data are available for Germany only. The parametrization in (b) is $\tau^* = 1400\,\mathrm{s}$, $f_{\mathrm{C_w}} = 1.0$, $f_{\mathrm{dry}} = 0.4$, and $c_{\mathrm{oro}} = 0.8$. The areas outside of Baden-Württemberg are covered white for better visualization and comparison.

best results in terms of the lowest rmse (Fig. 11) for higher stability (increase of N_{m}^2) or longer time scales, whereas in the case of water vapor density q_{v} or horizontal wind speed U, the lowest rmse is obtained when decreasing the original values. The results also reveal a higher sensitivity of the rSPM to changes in water vapor and wind speed for this event. Regarding wind direction β, the lowest rmse is given for the original value.

The highest skill score S, conversely, is reached for increasing U and q_{v}, and decreasing τ and N_{m}^2. In the case of wind direction, S continuously decreases from 0.8 in the northwesterly inflow to 0.4 in the northeasterly winds.

For the case study of 31 May 2013, the observed mean for Baden-Württemberg is $\bar{R}_{\mathrm{obs}} = 33.1$ mm, whereas the simulated mean is $\bar{R}_{\mathrm{mod}} = 37.3$ mm, and thus, only 12.6 % higher compared with the observations. The rmse and skill score S are near the optimum when perturbing different variables. The deviations of spatial means and quality indices are at a reasonable level. However, as already explained, the SPM2D is not designed to represent historic events in detail. Other parameter combinations of $f_{\mathrm{C_w}}$, f_{dry}, c_{oro} and τ^* may yield even better results for this single event.

5 Parameter estimation for the stochastic simulations

5.1 Adjustment of the distribution functions

Stochastic model simulations are based on pdfs that are adjusted to the required parameter. Event duration as well as background and frontal precipitation are estimated from REGNIE data for the top200 event set. Ambient parameters required by

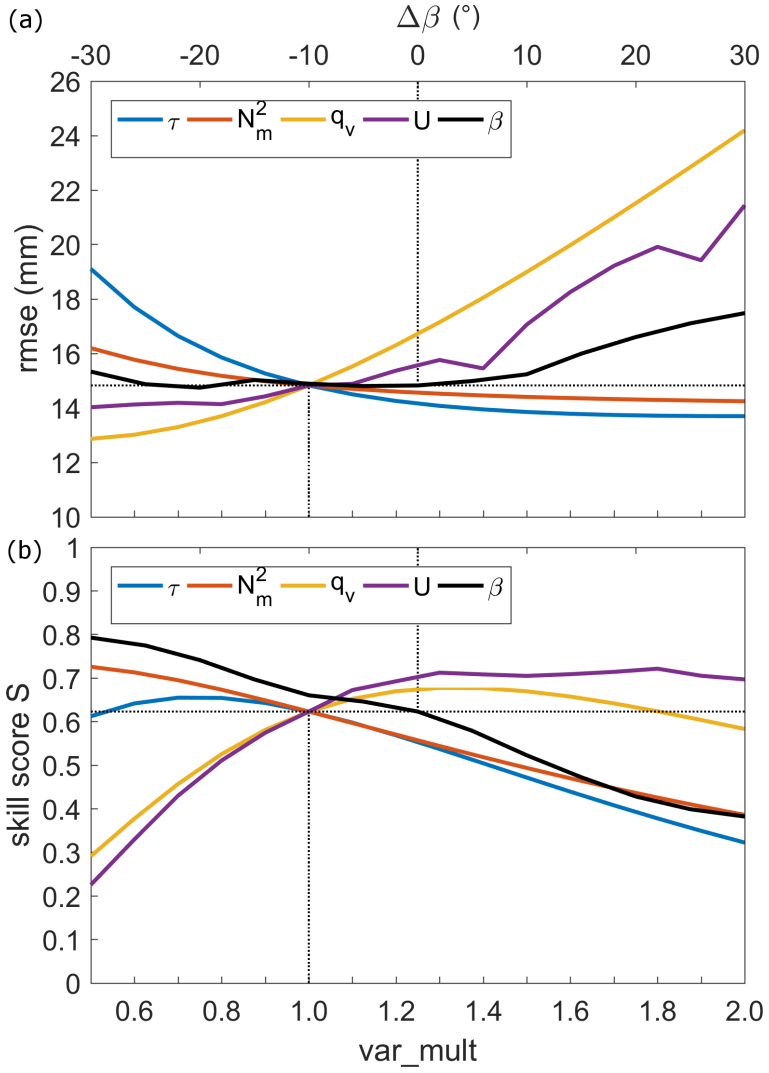

Figure 11. Changes of (a) rmse, and (b) skill score S for perturbed values of N_{m}^2, q_{v}, U, β, and τ, with a multiplicative factor (var_mult), and changed $\Delta\beta$, for 31 May, 2013. The dotted lines indicate the values of the reference run.

the SPM2D are derived from vertical profiles of the radiosondes at Stuttgart, whereas the extent of embedded convection is estimated from the radar tracks of severe convection. Furthermore, as mean ambient conditions and thus precipitation characteristics change throughout the year, we differentiate among the four seasons.

After separating the historic event set into the four main seasons, we estimate for each of the 10 parameters the pdf that best fits the distribution of the observations (= 10 parameters × 4 seasons = 40 cases; Table 3) by using the least QIRS method (cf. Sect. 2.6). From the overall 21 pdfs that were considered, only 12 are suitable for adjusting the observations. In most of the cases, the GEV with its special realizations of Gumbel (GbD) and Weibull (WbD) distribution appears to be appropriate (26

Table 3. Estimated best fitting pdfs for event duration (t_{ev}), background precipitation R_{∞}, and frontal enhancement factor c_{front} derived from REGNIE data (top box); square of saturated Brunt-Väisälä frequency N_{m}^2, wind direction β, horizontal wind speed U, water vapor scale height H_{w}, actual lapse rate γ, saturated moist adiabatic lapse rate Γ_{m}, and condensation rate $\rho_{\mathrm{S_{ref}}}$ derived from sounding data (bottom box); for the pdf aconyms: see Table 1.

model parameter	MAM	JJA	SON	DJF
t_{ev}	GEV	GEV	BSD	NkD
R_{∞}	WbD	WbD	WbD	WbD
c_{front}	LND	GmD	LND	ND
N_{m}^2	GEV	GbD	GEV	GEV
β	GEV	GEV	GEV	SD
U	HND	IGD	HND	GEV
γ	GEV	GEV	IGD	IGD
Γ_{m}	GEV	IGD	IGD	GEV
H_{w}	GEV	GbD	GEV	LD
$\rho_{\mathrm{S_{ref}}}$	WbD	GEV	WbD	WbD

distributions), followed by the inverse Gaussian pdf (IGD) for five parameters and the Gamma pdf (GmD) for three parameters. Especially for flow parameters derived from the soundings, GEV appears to be the most appropriate (19 out of 28 cases). In five out of 40 cases ($\approx 12.5\,\%$), we had to choose the pdf manually due to the alikeness of two pdfs according to the QIRS method.

The input parameters are considered as independent and uncorrelated. To justify this assumption, we perform a correlation analysis of all possible combinations of input parameters using the correlation coefficient of Spearman (1904). In total, a low number of about 16 % have a correlation coefficient above $\pm\,0.5$ and only 4 % are highly correlated with ± 0.7. Regarding these cases, 90 % show negative correlations with $r \leq -0.5$. However, there are distinct seasonal differences, for instance, with correlations in summer, but almost no correlation in winter regarding the same variables. The most frequent correlation exists between the saturated Brunt-Väisälä frequency N_{m}^2 and the lapse rates γ and Γ_{m}. Furthermore, as shown in Sect. 4, the SPM2D is less sensitive to N_{m}^2. Thus associated correlations have less influence.

5.2 Event characteristics

Based on REGNIE data and the method described in Sect. 2.6, we estimate for each event within top200 the duration t_{ev} (in days), again differentiating among the seasons. The histogram of historic events and the corresponding best-fitting pdf (Fig. 12) shows that during the summer (JJA), a duration of two to three days dominates with a decreasing probability toward longer periods. In the winter (DJF), the distribution is generally shifted to longer events, whereas the probability for single-day events remains roughly unchanged. The maximum of 15 days in DJF represents the longest duration of top200. Whereas the estimated

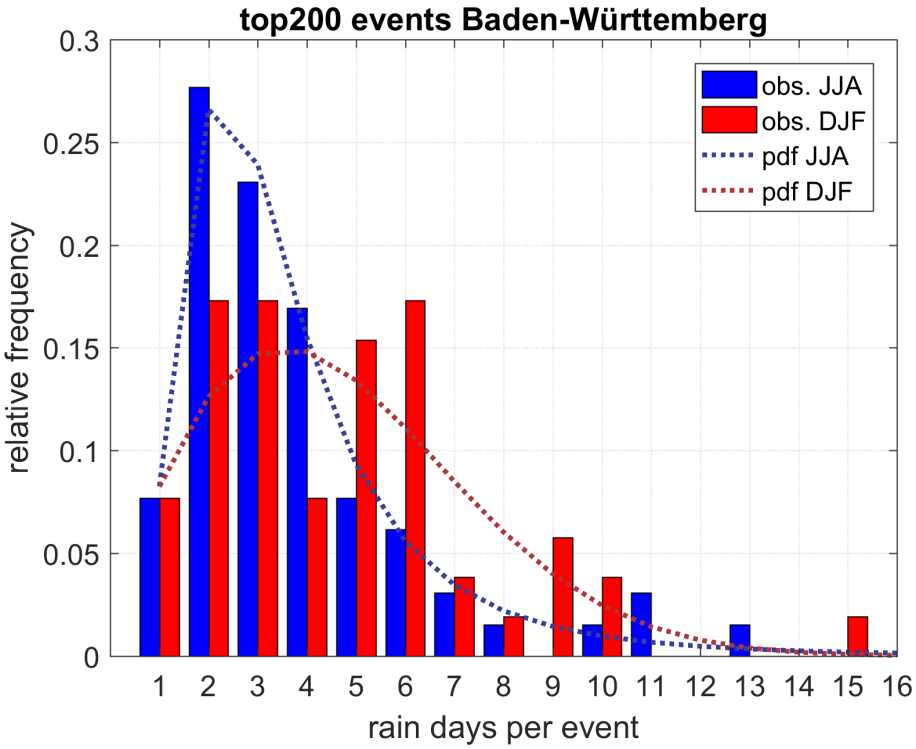

Figure 12. Histogram of top200 event duration for Baden-Württemberg according to REGNIE (bars), and estimated best fitting pdfs (dotted lines) for the summer (blue) and the winter (red).

pdf for the summer (GEV) has a sharper maximum and a stronger decrease for $t_{\mathrm{ev}} > 3$, the pdf found to best fit the duration in the winter (NkD) shows a broader range of possible durations. Note that the histogram in the winter shows a large scattering with irregular peaks, making an adjustment to a pdf very problematic. For spring and autumn, the results are comparable to those of winter and summer, respectively.

Concerning background precipitation R_{∞}, totals of 20–25 mm d^{-1} are found to most likely occur within a range of 3–37 mm d^{-1} in winter, 3–50 mm d^{-1} in summer, and 0–50 mm d^{-1} during the other two seasons (not shown). For all seasons, the Weibull distribution (WbD) is most appropriate. For frontal factor c_{front}, we obtain a log-normal distribution (LND) for spring and fall, a normal pdf (ND) for the winter, and a Gamma pdf (GmD) for the summer. All pdfs have their maximums around 0.7 to 0.8 with a range from 0.4 to 1.4 for most of the seasons (not shown). The gamma distribution in fall has a sharp ascent and a slower descent toward higher values (maximum of around 1.6).

5.3 Atmospheric parameters

As described in Sect. 2, orographic precipitation in the SPM2D depends on seven atmospheric parameters (cf. Table 3). An overview of the range of all parameters is shown as box plots in Fig. 13. In most cases, the atmosphere was slightly stably

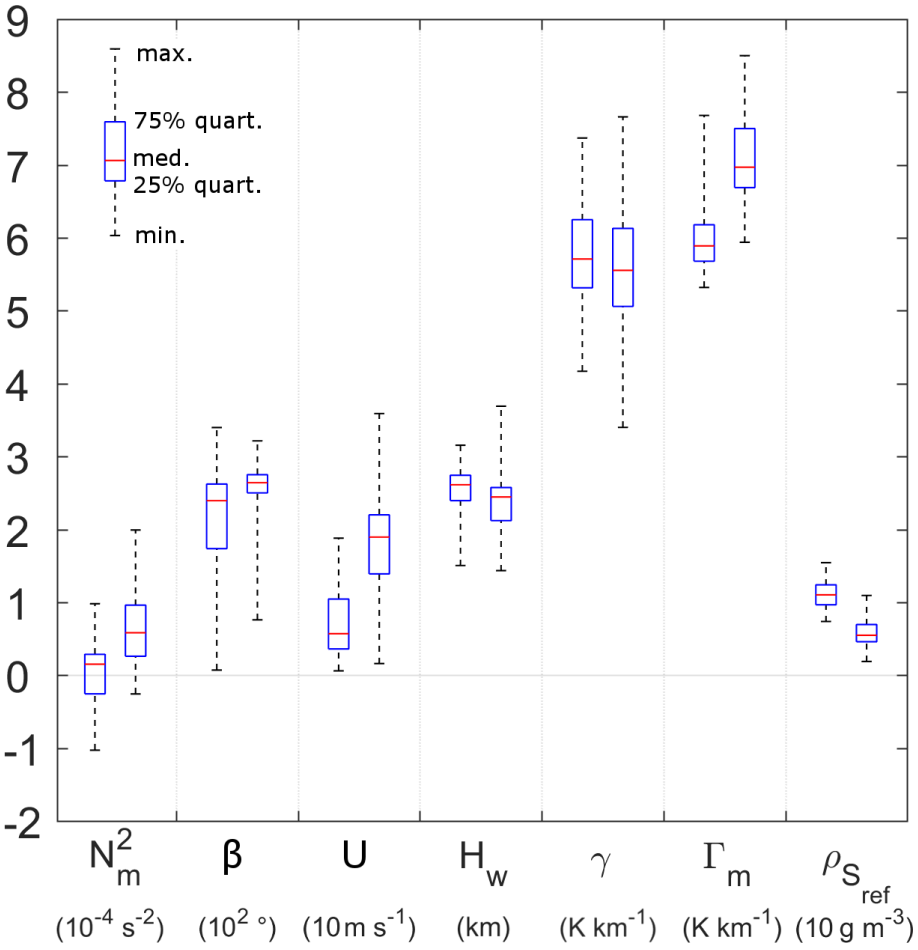

Figure 13. Atmospheric parameters required for the SPM2D derived from radiosounding observations at Stuttgart for top200 events with mean, interquartile distance, minimum, and maximum values; the left box-whisker of each pair represents the summer, the right one represents the winter season. The units for each variable are given in the brackets below the variable names.

stratified as represented by positive values of the squared Brunt-Väisälä frequency N_{m}^2 affecting the wave propagation. During summer, the distribution is shifted toward negative values (= unstable; recall that negative values are set to $N_{\mathrm{m}} = 0.0003\ \mathrm{s}^{-1}$), whereas in winter, there are almost entirely positive values. Wind direction β, decisive for the spatial distribution of precipitation around the mountains, shows pronounced seasonal differences. More than 90 % of the top200 winter events have southwesterly to northwesterly winds (240°–300°), with other directions hardly observed. The reason is that northerly flows are usually associated with low temperatures and thus low humidity during the winter and do not have the potential for heavy precipitation. In summer, the wind direction that occurred most frequently is between 240° and 300° as well. However, all other directions have been observed as well.

Horizontal wind speed U is high, especially during winter, where reduced moisture is compensated by high velocity to obtain substantial horizontal incoming moisture flow. Median values are 5 and 20 m s^{-1} during summer and winter respectively. Flow parameters related to humidity (H_{w}, $\rho_{\mathrm{S_{ref}}}$) conversely show higher values in summer, where Γ_{m} is reduced due to the release of latent heat. Observed vertical temperature gradients γ show similar medians and interquartile ranges with a broader distribution in winter.

6 Stochastic event set and model validation

Overall, a total number of $n_{\mathrm{E}} = 10{,}000$ events (approx. 31,500 days) have been simulated with SPM2D, hereafter referred to as SPM10k. The rSPM part of this event set is referred to as rSPM10k in the following section. For the validation of the SPM2D, we quantified statistical values, such as return periods, probabilities, or percentiles and evaluate them with observations (REGNIE), CCLM simulations and the rSPM results. Note that the main reference is the REGNIE top200 event set.

Spatial 24-hour mean values for the area of Baden-Württemberg range between 1.2 and 79.7 mm in SPM2D, and 1.3 to 97.0 mm in rSPM, whereas the maximum for top200 is only 49.6 mm. In total, 128 events (0.4 %) of SPM10k or 724 (2.1 %) of rSPM10k yield higher spatial precipitation amounts than the maximum of top200. The CCLM simulations range between 1.8 and 37.6 mm.

Both median and 90th-percentile (p90) precipitation fields of top200 events and the SPM10k agree well concerning the spatial distribution as well as the precipitation amounts (Figs. 14 and 15). Significant orographic structures in the precipitation fields over the Black Forest and Swabian Jura are clearly visible in all data sets. Note that the more detailed structure of REGNIE data results from the regionalization method and its strong dependency on orography and should not be over-interpreted. Larger spatial differences mainly appear in the northern parts of Baden-Württemberg (the Northern Rhine Valley and north-eastern rolling hills) for both the median and the p90 field, whereat for the latter, differences also arise in an additional area northeast and southwest of Stuttgart. Nevertheless, all differences are small in the order of a few percent. The rSPM shows an overestimation of precipitation especially over mountainous terrain, whereas the CCLM simulates overall less precipitation for the median. For the p90 field, major differences appear especially in low lands.

The areal rainfall of the SPM10k median field differs only about 3.3 % from top200, whereas that of the rSPM10k is about 22.1 % higher. The spatial mean precipitation of the CCLM reanalysis is barely half of REGNIE, which might be a result of the reduced sample size. The maximum values at any grid point for the median field are about 7 % higher in the SPM10k compared to top200, and about 34 % higher in the rSPM10k, whereas the CCLM maximum ist about 44 % smaller. The areal rainfall for the p90 field is about 6.5 % smaller in SPM10k, and about 14 % higher in rSPM10k, but about 22 % smaller in CCLM. The maximum values at any grid point for the p90 field is approximately 1 % smaller in SPM10k, and about 22 % higher in rSPM10k and 13 % higher in CCLM.

Comparing precipitation amounts for other percentiles, for example, between the 16th and 99th percentiles (Fig. 16 a), the differences between REGNIE and the SPM2D are very small for the spatial mean values and the maximum precipitation at any grid point in the model domain. The differences become considerable only for the 95th percentile and above. The SPM2D

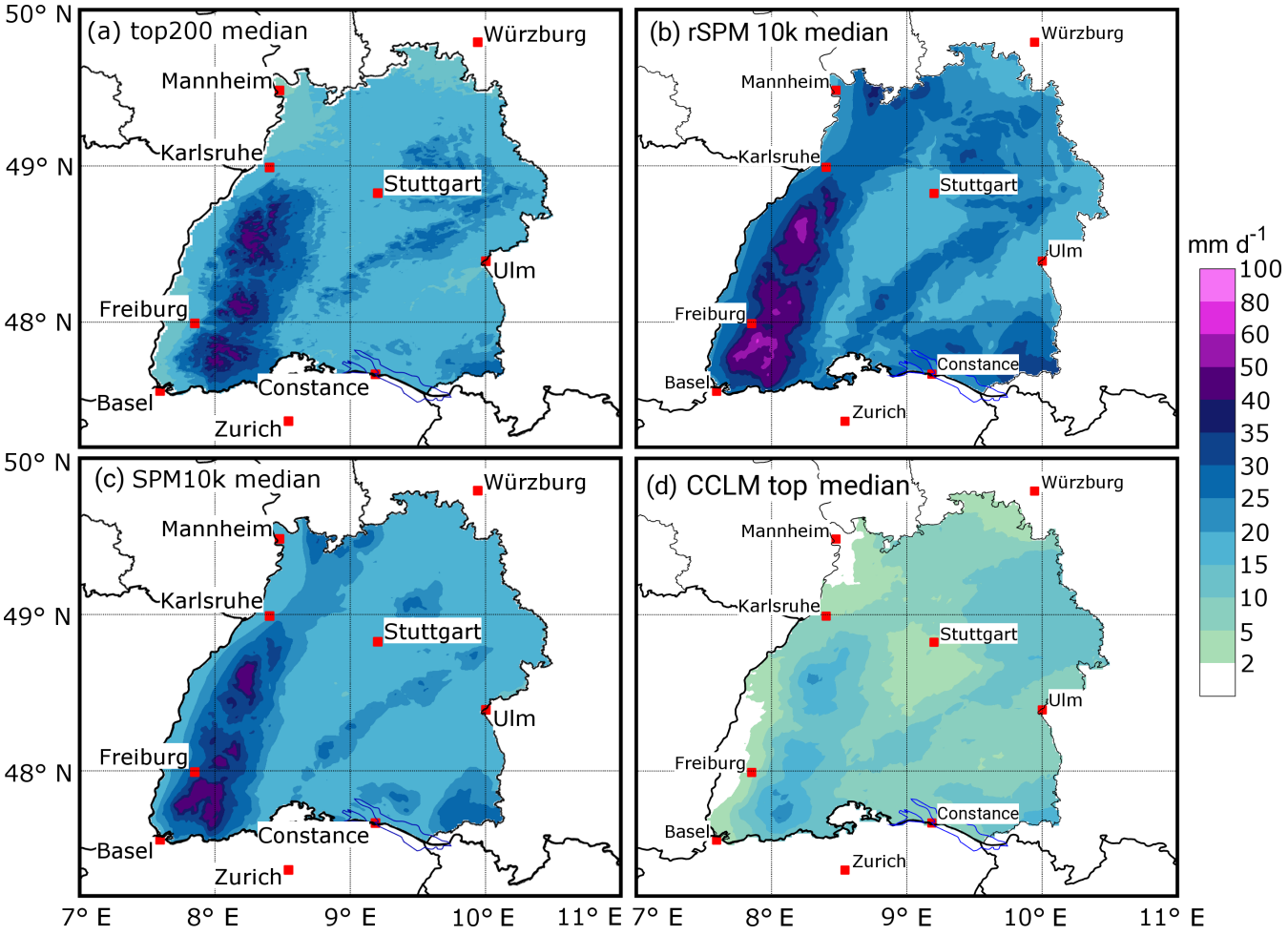

Figure 14. Precipitation fields for the median of (a) the top200 (REGNIE) events, (b) the rSPM10k, (c) the SPM10k , and (d) the CCLM simulations.

tends to overestimate lower precipitation amounts because the minimum values at any grid point are higher in the model than in the observations and invert for the 99th percentile only. In contrast, the differences between the rSPM and REGNIE are considerably larger for maxima, minima and spatial means throughout every percentile. The CCLM reanalysis has a negative deviation for minimum and spatial mean precipitation in all percentiles, whereas for the maximum values there is a marked underestimation for lower percentiles and an overestimation at higher percentiles.

At small percentiles, or for small precipitation amounts, respectively, QIs, such as correlation coefficient r, skill score S, and normalized standard deviation $\hat{\sigma}_{\mathrm{f}}$, have low values due to the overestimation of the SPM2D (Fig. 16 b). The highest skill is reached around the 90th percentile with a slight decrease for higher values, which can be the result of the increasing uncertainties of the observations. Nevertheless, a skill score of around or above 0.8 confirms the reliability of the simulations.

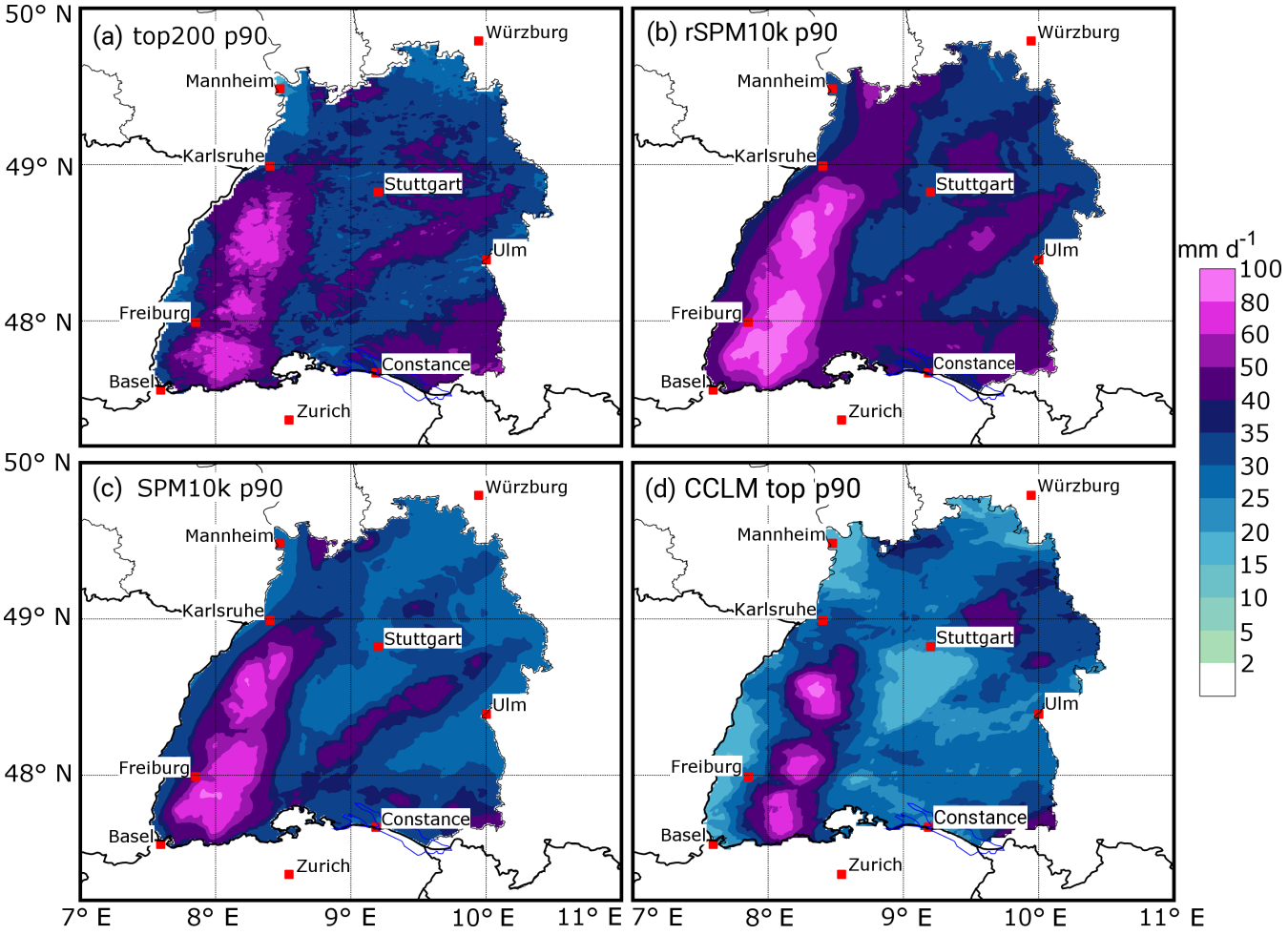

Figure 15. Precipitation fields for the 90th percentile (p90) of (a) the top200 (REGNIE) events, (b) the rSPM10k, (c) the SPM10k, and (d) the CCLM simulations.

Note that the QIs describe the performance of the SPM2D compared to REGNIE solely. In the following we concentrate our analysis on SPM2D and REGNIE.

To estimate precipitation distributions for specific return periods, we fit a Gumbel distribution (Wilks, 2006) to the annual maximum series of both REGNIE and the SPM10k. As it is not possible to estimate the time period and a corresponding annual maximum series for the stochastic event set, we count the number of stochastic values exceeding the 99th percentile of observations $n_{\mathrm{p}_{99}}$ and normalize it by the probability of occurrence p_{99}, giving the new time period T_{SPM}:

$$T_{\mathrm{SPM}} = \frac{n_{\mathrm{p}_{99}}}{p_{99}}\,. \tag{13}$$

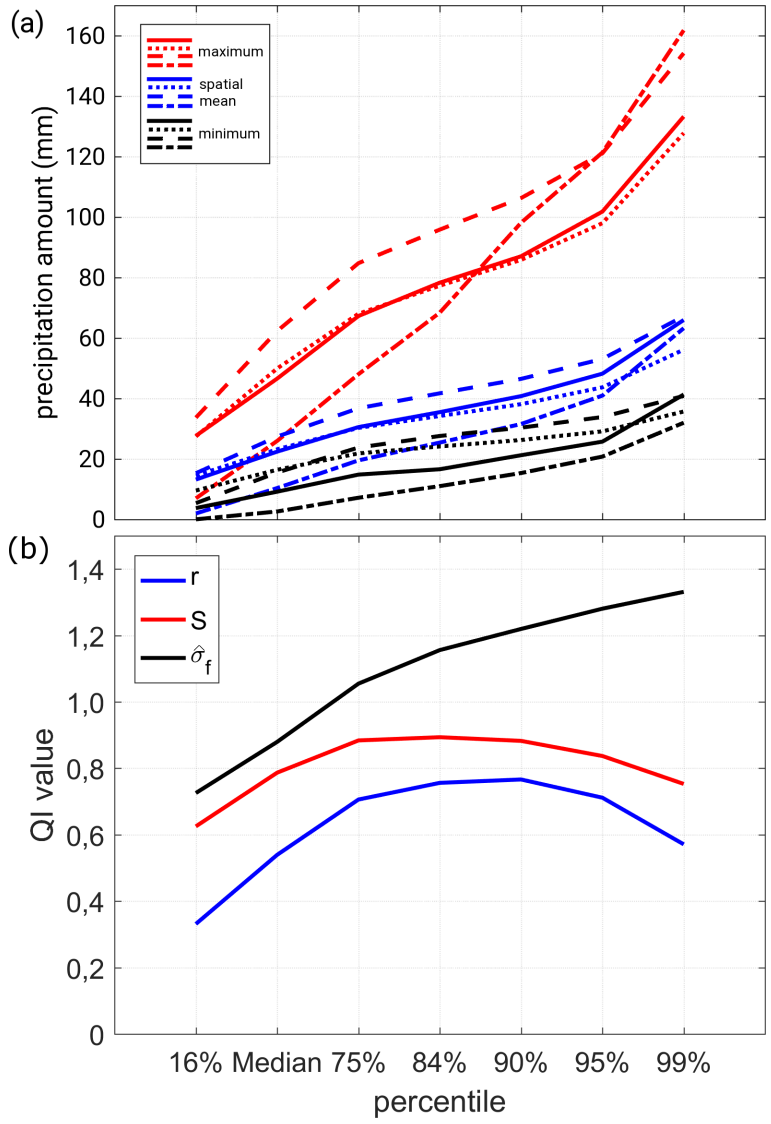

Figure 16. Comparison of (a) the maximum (red), the minimum (black), and the spatial mean precipitation (blue) of REGNIE (solid line), the SPM2D (dotted line), the rSPM (dashed line) and CCLM simulations (dot-dashed line), and (b) quality indices (QI) r, S, and $\hat{\sigma}_{\mathrm{f}}$ for different percentiles of the SPM2D compared to REGNIE.

After sorting the SPM10k in descending order, we take the first $n_T = T_{\mathrm{SPM}}$ values as the annual series of the SPM10k and estimate a new Gumbel distribution. Using these distributions, we obtain precipitation values for specific return periods for both the observations and the SPM10k. This method is applied to the spatial mean values of different areas and for every single grid point.

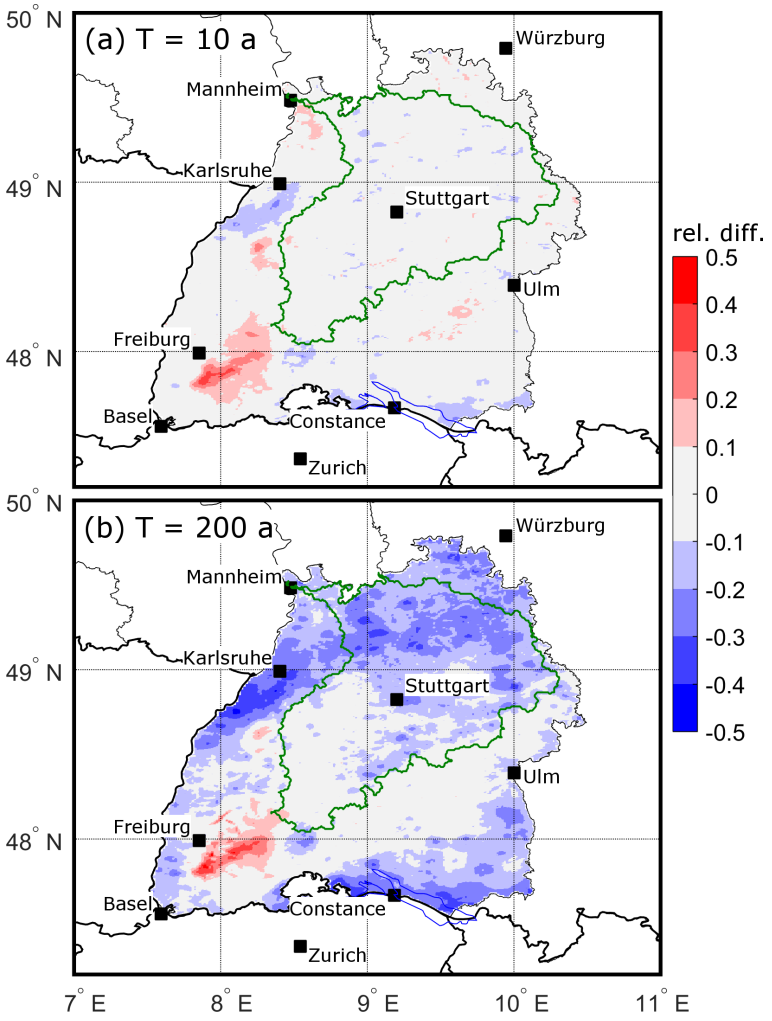

Figure 17. Relative difference of the precipitation amounts for (a) a return period of $T = 10$ years, and (b) $T = 200$ years, according to a Gumbel distribution fitted to the observations (top200) and the SPM10k (see text for further explanation). The Neckar catchment is shown as green contour.

For a 10-year return period, the SPM10k shows only small deviations from REGNIE of less than $\pm 10\,\%$ over almost the entire area of Baden-Württemberg, with a small area of overestimation in the Southern Black Forest (Fig. 17 a). The areal mean difference is only 0.6 %. In the case of $T = 200$ yrs (Fig. 17 b), the overestimation in the Southern Black Forest remains with almost the same relative discrepancy. For this return period, the SPM10k tends to underestimate precipitation, especially in the northern part of Baden-Württemberg and in the southeast around Lake Constance. Nevertheless, the deviations for most of the grid points are between $\pm 20\,\%$, and the areal mean difference is about –10 %. Taking into account the strongly increasing uncertainties of the observed values for higher return periods, especially for $T > 100$ years, this is still a reasonable result.

On the level of the major river catchments, the differences are small, too. For the Neckar catchment, for example (see Fig. 17), which covers about 38 % of Baden-Württemberg, the spatial mean deviation is about –0.5 % in the case of $T = 10$ yrs and –12.7 % for the 200-year return period. Even for the catchments containing the area of overestimation in the Southern Black Forest (Upper Rhine between Basel and Mannheim, and High Rhine between Constance and Basel), the spatial mean deviations are between +1 and +4 % for $T = 10$ yrs and between –2 and –10 % for $T = 200$ yrs respectively.

Single grid point deviations and the ensuing spatial mean values as described above are sensitive to local conditions and uncertainties in both REGNIE and SPM10k data. Hence, we evaluate the model in a similar way by calculating the spatial mean precipitation first and then fitting a Gumbel distribution to the spatial means in a second step. For the plotting, return period T_k of each element x_k of the annual maximum series with length T_{max} is given by $T_k = T_{max} \cdot \mathrm{rk}^{-1}(x_k)$ with the rank $\mathrm{rk}(x_k)$ of element x_k (annual series sorted in descending order). The first element (highest value) of an annual series of, for example, 100 years therefore has a return period of $T_1 = 100$ yrs, the second $T_2 = 50$ yrs, and so on. The values of T_k were adjusted using the plotting position method of Cunnane (1978).

Again, the difference between the simulated and observed spatial mean values of daily precipitation for the whole of Baden-Württemberg is small, with slightly lower values from the simulations (Fig. 18 a). The distribution of the SPM10k is very close and almost parallel to the estimated observed Gumbel distribution and within the 95 % confidence interval (CI95) estimated with the formula of Maity (2018). Considerable differences between the SPM10k and REGNIE arise only for return periods of $T = 1000$ yrs and above but are still small. For the Neckar catchment, the simulation results agree well with the observed distribution for return periods up to approximately 300 years (Fig. 18 b). For higher return periods, the differences increase but are still inside the CI95. Similar results can be found for other river catchments. Note again that for such high return values, the statistical uncertainty of the observed distribution also increases significantly.

7 Summary and Conclusions

We have presented a novel method for estimating the statistics of total rainfall based on a stochastic model approach (SPM2D). Total precipitation at each grid point is calculated from the linear superposition of four different parts: orographic precipitation, synoptic background precipitation, frontal precipitation and precipitation from convection embedded into stratiform clouds. The linear theory of orographic precipitation according to Smith and Barstad (2004), which represents the core of the SPM2D, has been modified using three different calibration parameters to minimize the weaknesses found in previous studies such as the overestimation of wave dynamics and, thus, resulting precipitation and evaporation (e. g., Barstad and Smith, 2005; Kunz, 2011). For cross-validation, we calibrated and adjusted the SPM2D to a historic event set of heavy rainfall events (top200; training data). By adjusting appropriate probability density functions (pdfs) for all required model parameters, we simulated 10,000 independent stochastic precipitation events (validation data). The results were compared with observations and reanalysis data using different percentiles and return periods.

The focus of the presented investigations was on the Federal State of Baden-Württemberg in Southwest Germany with the striking low-mountain ranges of Black Forest and Swabian Jura. The following main conclusions can be drawn:

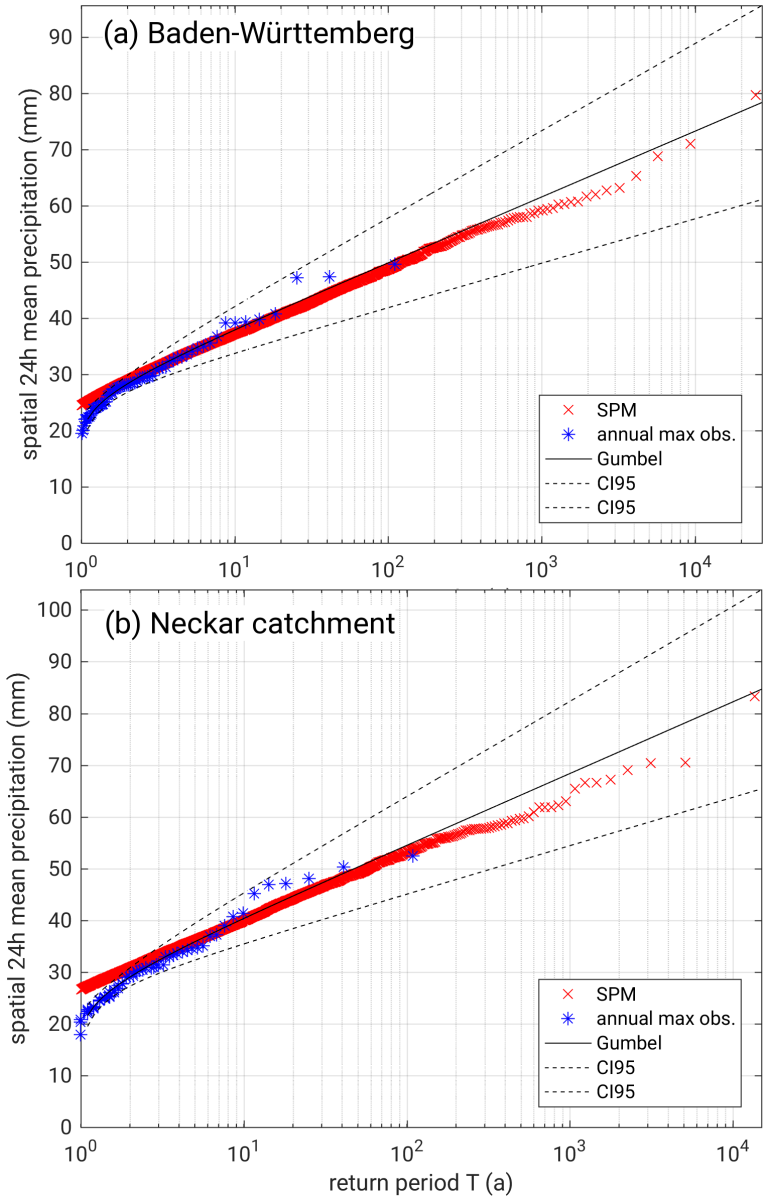

Figure 18. Daily rainfall totals (areal mean) as a function of return period T based on the annual maximum series of observations (REGNIE, blue), the corresponding Gumbel distribution including the 95 % confidence intervals (black), and the annual SPM10k series (red) for (a) the Federal State of Baden-Württemberg, and (b) the Neckar catchment.

– The SPM2D has a high skill to simulate both historic and stochastic heavy rainfall events. The simulated spatial distributions and magnitudes are reliable despite the simplified approach of the model initialized by a set of atmospheric variables obtained from radiosoundings. The differences between the SPM2D and REGNIE are small with deviations of

less than 10 %. Local differences, however, may also be traced back to uncertainties in REGNIE observations, mainly because of prevailing inhomogeneities in the spatial distribution of rain gauges, especially over mountainous terrain.

- The comparison of the SPM2D with the reduced stochastic model rSPM demonstrates the need to additionally consider precipitation related to frontal systems and embedded convection. The SPM2D with simplified parameterizations for these parts even yields more reliable precipitation fields for a historic event set compared to the sophisticated high-resolution NWP model CCLM.

- The solution of the model equations in Fourier space by an FFT allows for the simulation of a large number of events and to run the model in stochastic mode.

- The extent of the model domain has to be limited to ensure the validity of the assumption of spatially homogeneous distributed atmospheric conditions and synoptic forcing. This allows, for instance, for the usage of a vertical profile from a single radiosounding station (or model data).

- The presented stochastic approach is easily applicable to other investigation areas. Atmospheric variables for the initialization of the model can be estimated either from radiosoundings as within this study or using reanalysis or data from NWP models. Therefore, it can be applied to any region of the world with similar precipitation characteristics even if there is only a limited number of ground-based observations available.

As shown in our study, the SPM2D is sensitive to perturbations of ambient conditions. Therefore, high-quality input data, especially of the atmospheric parameters, are essential. On the other hand, the sensitivities of precipitation and rmse to changing input parameters is limited in a range of around $\pm 10\%$ of the original values, which is usually within the range of uncertainty. Using data of only one sounding station turned out to be sufficient to achieve reliable heavy rainfall fields. As shown by (Kunz, 2011), the differences to another upstream sounding station (Nancy in France) are small, at least in the mean. This, however, applies only for widespread precipitation with durations over several hours to days, which is the focus of our study. Intermittent or even mainly convectively-driven events cannot be reliably reproduced by our model.

The input parameters can be considered as independent, as just a few cases revealed higher correlation. The sensitivity of the model for these parameters, however, turned out to be week. Additionally, the correlation coefficients between the model input parameters vary among the seasons.

To transfer the method to another investigation area, just a few steps are necessary: first a proper sample of historical heavy rainfall events. In the next step, the statistics (pdfs) of the prevailing ambient conditions, background precipitation, and duration for the event set have to be calculated. Finally, the reduced SPM (rSPM) has to be calibrated by determining appropriate values for the free model tuning parameters.

The presented SPM2D is part of the project FLORIS (Flood Risk), which represents a novel risk assessment methodology for an entire domain and not only for single catchments applied in the insurance industry. Within the framework of this project, the SPM2D was applied to other federal states in central Germany. The modeled precipitation fields are used as input data for hydrological and hydraulic simulations, from which the flood risk can be estimated, for example for a one-in-200-years event

required according to the insurance regulation of Solvency II. However, the results of the SPM2D basically can be used for several different applications such as water management or the design of flood protection measures.

8 Data availability

The REGNIE data used in this paper are freely available for research and can be requested at the DWD (doi:10.1127/0941-2948/2013/0436); The sounding data are freely available from the Integrated Global Radiosonde Archive (https://www.ncdc.noaa.gov/data-access/weather-balloon/integrated-global-radiosonde-archive). The required orographic data can be obtained from http://srtm.csi.cgiar.org/ (doi:10.1080/13658810601169899).

Competing interests. The authors declare that they have no conflict of interest.

Acknowledgements. The authors thank a local insurance company for funding the project. We also would like to thank the German Weather Service (DWD) and the Integrated Global Radiosonde Archive (IGRA) for providing different observational data sets and CGIAR-CSI for the orographic data. Special thanks go to James Daniell, Andreas Kron and Simon Hoellering from KIT for constructive discussions within the project and for valuable suggestions during the model development. We acknowledge support by Deutsche Forschungsgemeinschaft (DFG) and open access publishing fund of Karlsruhe Institute of Technology (KIT). We are grateful to the constructive comments and suggestions of three anonymous reviewers that helped to improve the quality of this paper.

References

Barstad, I. and Caroletti, G. N.: Orographic precipitation across an island in southern Norway: model evaluation of time-step precipitation, Q. J. R. Meteorol. Soc., 139, 1555–1565, 2013.

Barstad, I. and Smith, R. B.: Evaluation of an Orographic Precipitation Model, J. Hydrometeorol., 6, 85–99, 2005.

Basist, A., Bell, G. D., and Meentmeyer, V.: Statistical relationships between topography and precipitation patterns, J. Climate, 7, 1305–1315, 1994.

Bergeron, T.: On the physics of fronts, Bull. Am. Meteorol. Soc., 18, 265–275, 1937.

Browning, K. A., Pardoe, C. W., and Hill, F. F.: The nature of orographic rain at wintertime cold fronts, Q. J. R. Meteorol. Soc., 101, 333–352, 1975.

Cannon, D. J., Kirshbaum, D. J., and Gray, S. L.: Under what conditions does embedded convection enhance orographic precipitation?, Q. J. R. Meteorol. Soc., 138, 391–406, 2012.

Caroletti, G. N. and Barstad, I.: An assessment of future extreme precipitation in western Norway using a linear model, Hydrol. Earth Syst. Sci., 14, 2329–2341, 2010.

Crochet, P., Jóhannesson, T., Jónsson, T., Sigurdsson, O., Björnsson, H., Pálsson, F., and Barstad, I.: Estimating the spatial distribution of precipitation in Iceland using a linear model of orographic precipitation, J. Hydrometeorol., 8, 1285–1306, 2007.

Cross, D., Onof, C., Winter, H., and Bernardara, P.: Censored rainfall modelling for estimation of fine-scale extremes, Hydrol. Earth Syst. Sci. Discuss., https://doi.org/10.5194/hess-2017-437, 2017.

Cunnane, C.: Unbiased plotting positions – a review, J. Hydrol., 37, 205–222, 1978.

Drogue, G., Humbert, J., Deraisme, J., Mahr, N., and Freslon, N.: A statistical-topographic model using an omnidirectional parameterization of the relief for mapping orographic rainfall, Int. J. Climatol., 22, 599–613, https://doi.org/10.1002/joc.671, 2002.

Duckstein, L., Bárdossy, A., and Bogárdi, I.: Linkage between the occurrence of daily atmospheric circulation patterns and floods: an Arizona case study, J. Hydrol., 143, 413–428, 1993.

Durran, D. R. and Klemp, J. B.: On the effects of moisture on the Brunt-Väisälä frequency, J. Atmos. Sci., 39, 2152–2158, 1982.

Durre, I., Vose, R. S., and Wuertz, D. B.: Overview of the integrated global radiosonde archive, J. Climate, 1151, 53–68, 2006.

Eliassen, A.: On the vertical circulation in frontal zones, Geophys. Publ., 24, 147–160, 1962.

Fluck, E.: Hail statistics for European countries, Phd thesis, Institute of Meteorology and Climate Research (IMK), Karlsruhe Institute of Technologie (KIT), Karlsruhe, Germany, https://doi.org/10.5445/IR/1000080663, 2018.

Freedman, D. and Diaconis, P.: On the histogram as a density estimator: L2 theory, Zeitschrift für Wahrscheinlichkeitstheorie und Verwandte Gebiete, 57, 453–476, https://doi.org/10.1007/BF01025868, 1981.

Fuhrer, O. and Schär, C.: Embedded cellular convection in moist flow past topography, J. Atmos. Sci., 62, 2810–2828, 2005.

Furrer, E. M. and Katz, R. W.: Generalized linear modeling approach to stoachstic weather generators, Clim. Res., 34, 129–144, 2007.

Goovaerts, P.: Geostatistical approaches for incorporating elevation into the spatial interpolation of rainfall, J. Hydrol., 228, 113–129, 2000.

Handwerker, J.: Cell tracking with TRACE3D - a new algorithm, Atmos. Res., 61, 15–34, 2002.

Houze, R. A. and Hobbs, P. V.: Organization and Structure of Precipitation cloud systems, Adv. Geophys., 24, 225–315, 1982.

Jiang, Q. and Smith, R. B.: Cloud timescales and orographic precipitation, J. Atmos. Sci., 60, 1543–1559, 2003.

Kållberg, P., Simmons, A., Uppala, S., and Fuentes, M.: The ERA-40 archive. [Revised October 2007], Shinfield Park, Reading, 2004.

Kienzler, S., Pech, I., Kreibich, H., Müller, M., and Thieken, A. H.: After the extreme flood in 2002: changes in preparedness, response and recovery of flood-affected residents in Germany between 2005 and 2011, Nat. Hazards Earth Syst. Sci., 15, 505–526, 2015.

Kirshbaum, D. J. and Durran, D. R.: Factors governing cellular convection in orographic precipitation, J. Atmos. Sci., 61, 682–698, 2004.

Kirshbaum, D. J. and Smith, R. B.: Temperature and moist-stability effects on midlatitude orographic precipitation, Q. J. R. Meteorol. Soc., 134, 1183–1199, https://doi.org/10.1002/qj.274, 2008.

Koutsoyiannis, D., Kozonis, D., and Manetas, A.: A mathematical framework for studying rainfall intensity-duration-frequency relationships, J. Hydrol., 206, 118–135, 1998.

Kunz, M.: Characterisitics of Large-Scale Orographic Precipitation in a Linear Perspective, J. Hydrometeorol., 12, 27–44, 2011.

Kunz, M. and Wassermann, S.: Moist dynamics and sensitivity of orographic precipitation to changing ambient conditions in an idealised perspective, Meteorol. Z., 20, 199–215, 2011.

Lalas, D. P. and Einaudi, F.: On the stability of a moist atmosphere in the presence of a background wind, J. Atmos. Sci., 30, 795–800, 1973.

Laube, N.: personal correspondence, Phd thesis, Institute of Meteorology and Climate Research (IMK), Karlsruhe Institute of Technologie (KIT), Karlsruhe, Germany, 2018.

Maity, R.: Statistical Methods in Hydrology and Hydroclimatology, Springer Nature Singapore Pte Ltd., https://doi.org/10.1007/978-981-10-8779-0, 2018.

Mardia, K. V. and Zemroch, P. J.: Algorithm AS 86: The Von Mises Distribution Function, Journal of the Royal Statistical Society. Series C (Applied Statistics), 24, 268–272, 1975.

Mason, B.: The physics of clouds, Oxford University Press, 671 pp., 1971.

MATLAB: MATLAB and Statistics Toolbox Release 2016b, (version 9.1), The MathWork Inc., Natick, Massachusetts, USA, http://de.mathworks.com/help/, last visited 10 August 2017, 2016.

Mohr, S. and Kunz, M.: Recent trends and variabilities of convective parameters relevant for hail events in Germany and Europe, Atmos. Res., 123, 211–228, 2013.

MunichRe: NatCatSERVICE, natcatservice.munichre.com/, accessed: 28 Sept 2017, 2017.

Neykov, N. M., Neytchev, P. N., and Zucchini, W.: Stochstic daily precipitation model with a heavy-tailed component, Nat. Hazards Earth Syst. Sci., 14, 2321–2335, https://doi.org/10.5194/nhess-14-2321-2014, 2014.

Palutikov, J. P., Brabson, B., Lister, D. H., and Adcock, S. T.: A review of methods to calculate extreme wind speeds, Meteorol. Appl., 6, 119–132, 1999.

Petrow, T., Zimmer, J., and Merz, B.: Changes in the flood hazard in Germany through changing frequency and persistence of circulation patterns, Nat. Hazards Earth Syst. Sci., 9, 1409, 2009.

Piper, D., Kunz, M., Ehmele, F., Mohr, S., Mühr, B., Kron, A., and Daniell, J.: Exceptional sequence of severe thunderstorms and related flash floods in May and June 2016 in Germany-Part 1: Meteorological background, Nat. Hazards Earth Syst. Sci., 16, 2835, 2016.

Rauthe, M., Steiner, H., Riediger, U., A., M., and Gratzki, A.: A Central European precipitation climatology - Part I: Generation and validation of a high-resolution gridded daily data set (HYRAS), Meteorol. Z., 22, 235–256, 2013.

Richardson, C. W.: Stochastic Simulation of Daily Precipitation, Temperature, and Solar Radiation, Water Resour. Res., 17, 182–190, 1981.

Rockel, B., Will, A., and Hense, A.: The regional climate model COSMO-CLM (CCLM), Meteorol. Z., 17, 347–348, 2008.

Schröter, K., Kunz, M., Elmer, F., Mühr, B., and Merz, B.: What made the June 2013 flood in Germany an exceptional event? A hydro-meteorological evaluation, Hydrol. Earth Syst. Sci., 19, 309–327, 2015.

Smith, R. B.: Linear theory of stratified hydrostatic flow past an isolated mountain, Tellus, 32, 348–364, 1980.

Smith, R. B.: Hydrostatic airflow over mountains, Adv. Geophys., 31, 1–41, 1989.

Smith, R. B. and Barstad, I.: A Linear Theory of Orographic Precipitation, J. Atmos. Sci., 61, 1377–1391, 2004.

Spearman, C.: The Proof and Measurement of Association between Two Things, The American Journal of Psychology, 15, 72–101, 1904.

Taylor, K. E.: Summarizing multiple aspects of model performance in a single diagram, J. Geophys. Res., 106, 7183–7192, 2001.

Uhlemann, S., Thieken, A. H., and Merz, B.: A consistent set of trans-basin floods in Germany between 1952-2002, Hydrol. Earth Syst. Sci., 14, 1277, 2010.

Wanner, H., Rickli, R., Salvisberg, E., Schmutz, C., and Schüepp, M.: Global climate change and variability and its influence on alpine climate-concepts and observations, Theor. Appl. Climatol., 58, 221–243, 1997.

Wilks, D. S.: Statistical Methods in the Atmospheric Sciences, vol. 91 of *International Geophysics Series*, Academie Press, San Diego, California, USA, 2nd edn., 2006.